CATALOG OF ULTRA-DIFFUSE GALAXIES IN THE COMA CLUSTERS FROM SUBARU IMAGING DATA[*]

MASAFUMI YAGI[1,2], JIN KODA[3,4,5], YUTAKA KOMIYAMA[1,6], AND HITOMO YAMANOI[1]

[1] Optical and Infrared Astronomy Division, National Astronomical Observatory of Japan, 2-21-1, Osawa, Mitaka, Tokyo, 181-8588, Japan; Yagi.Masafumi@nao.ac.jp
[2] Graduate School of Science and Engineering, Hosei University, 3-7-2, Kajinocho, Koganei, Tokyo, 184-8584 Japan
[3] Department of Physics and Astronomy, Stony Brook University, Stony Brook, NY 11794-3800, USA
[4] California Institute of Technology, MC 249-17, 1200 East California Boulevard, Pasadena, CA 91125, USA
[5] Chile Observatory, National Astronomical Observatory of Japan, Joaquín Montero 3000 Oficina 702, Vitacura, Santiago 763-0409, Chile
[6] SOKENDAI (The Graduate University for Advanced Studies), Mitaka, Tokyo 181-8588, Japan

ABSTRACT

We present a catalog of ultra-diffuse galaxies (UDGs) in the Coma cluster. UDGs are a subset of low surface brightness (SB) galaxies with very large effective radii defined by van Dokkum et al. We surveyed the Subaru data archive for deep Suprime-Cam/Subaru R-band images, and used data covering the $1°.7 \times 2°.7$ region of the Coma cluster. The data are ~1 magnitude deeper than the data of van Dokkum et al (2015a) in limiting SB. This paper explains the details of our sample selection procedure. This UDG catalog includes positions, magnitudes, effective radii, mean and central SBs, and colors (when available). Comparisons with previous galaxy catalogs in the literature are performed, and we show that the current catalog is the largest for UDGs. We also discuss that most of the UDGs are members of the Coma cluster, and the major axis of the UDGs tends to align toward the cluster center (radial alignment).

1. INTRODUCTION

An ultra-diffuse galaxy (UDG; van Dokkum et al. 2015a) is a newly defined type of galaxy, characterized by its large size and low surface brightness (SB). In the pioneering study, van Dokkum et al. (2015a) defined UDGs from their observation with the Dragonfly (DF) telescope array (Abraham & van Dokkum 2014) as having effective radius $r_e \gtrsim 1.5$ kpc and central SB $\mu_0 \gtrsim 24$ g-band mag arcsec^{-2}, and reported 47 UDGs (DF-UDGs) in the Coma cluster. Despite their small stellar masses, ~1/1000 of the Milky Way (MW), many of the DF-UDGs are as large as the MW in r_e. Therefore, they are "ultra-diffuse." Stimulated by this work, Koda et al. (2015) revisited the Coma cluster data (Okabe et al. 2014) obtained with the Subaru Prime Focus Camera (Suprime-Cam; Miyazaki et al. 2002) on the Subaru telescope (Iye et al. 2004). They found that all DF-UDGs in the Subaru data have high signal-to-noise ratio (S/N) and are spatially well resolved. Subaru imaging thus permits an investigation of their properties including fainter UDGs. Koda et al. (2015) reported 854 Subaru-UDGs in the archival Subaru data. Recently, UDGs are also reported in the Virgo cluster (Mihos et al. 2015; Boselli et al. 2016) and in the Fornax cluster (Muñoz et al. 2015). It suggests that UDGs could be a ubiquitous population in cluster environment.

By definition, UDGs are a subset of low surface brightness galaxies (LSBs), and LSBs in various environments that have been studied for decades. We surveyed the literature to find that some of the previous catalogs of LSBs include galaxies that satisfy the size and the SB criteria of UDGs (Sandage & Binggeli 1984; Bothun et al. 1987; Davies et al. 1988, 1989; Impey et al. 1988; McGaugh & Bothun 1994; Dalcanton et al. 1997; O'Neil et al. 1997, 1999; Binggeli & Jerjen 1998;

Carrasco et al. 2001, 2006; Bergmann et al. 2003; Kniazev et al. 2004; Gavazzi et al. 2005; Hunter & Elmegreen 2006; Misgeld et al. 2008; Buzzoni et al. 2012; Lieder et al. 2012; McConnachie 2012; Calderón et al. 2015; Makarov et al. 2015). These possible UDGs in the literature are summarized in Appendix B.

The large population and centrally concentrated distribution of the Subaru-UDGs in the Coma cluster (Koda et al. 2015) suggests their longevity. Most of the UDGs appear as smooth and relaxed systems (Koda et al. 2015; van Dokkum et al. 2015a), and have the color of quiescent galaxies (Koda et al. 2015). The tidal force of the cluster would exert strongly on the UDGs due to their large sizes, and require large internal masses, more than the measured stellar masses, and associated inward gravity for their survival. The dark matter fraction of UDGs in the Coma cluster are estimated as >98% (van Dokkum et al. 2015a) and >99% (Koda et al. 2015). Though their dynamical masses have not yet been measured directly, the above consideration suggests them to be a kind of hypothesized "dark galaxy," i.e., galaxies without much light for their masses (Trentham et al. 2001). The importance of dark matter in faint dwarf galaxies in a cluster environment was discussed by Penny et al. (2009). They showed that 12 out of the 25 dwarfs in their sample require dark matter to remain stable against the cluster potential. UDGs may be an important keystone for understanding galaxy formation and galactic dark matter in a cluster environment.

In this paper, we describe the detailed selection process of the UDGs published in Koda et al. (2015), and present the catalog of the Subaru-UDGs. The AB magnitude system of the instrument is used unless otherwise noted. We adopted cosmological parameters of $(h_0, \Omega_M, \Omega_\lambda) = (0.697, 0.282, 0.718)$ (Hinshaw et al. 2013), and a distance modulus of the Coma cluster of $(m - M)_0 = 35.05$ (Kavelaars et al. 2000). The angular diameter distance is 97.65 Mpc, and 1 arcsec corresponds to 0.473 kpc.

---

[*] Based on data collected at Subaru Telescope, which is operated by the National Astronomical Observatory of Japan.

Table 1
List of Fields

field	R.A.(J2000.)	Decl.(J2000.)	Exptime (minutes)	$\mu(2'')^a$	Seeing($''$)	Obsdate
COMA10	13:01:22.450	+26:57:19.06	24.5	28.5	0.9	2011 Apr 01
COMA11	13:01:23.225	+27:28:19.28	28	28.6	0.7	2011 Apr 01
COMA12	13:01:23.975	+27:59:20.23	24.5	28.3	0.6	2011 Apr 01
COMA13	13:01:24.754	+28:30:20.79	24.5	28.6	0.6	2011 Apr 01
COMA14	13:01:25.522	+29:01:22.30	24.5	28.5	0.7	2011 Apr 01
COMA20	12:59:34.993	+26:57:30.81	24.5	28.5	0.8	2011 Mar 02
COMA21	12:59:35.213	+27:28:33.54	52.5	28.5	0.6	2011 Mar 02, 2011 Mar 31
COMA22	12:59:36.374	+27:59:32.13	31.5	27.8	0.7	2011 Mar 02, 2011 Mar 31
COMA23	12:59:36.879	+28:30:31.19	24.5	28.4	0.7	2011 Mar 02
COMA24	12:59:37.452	+29:01:24.99	24.5	28.7	0.6	2011 Mar 02
COMA30	12:57:45.736	+26:57:35.08	49	28.6	0.7	2011 Mar 02, 2011 Mar 31
COMA31	12:57:46.785	+27:28:35.00	133	28.4	0.6	2011 Mar 02, 2011 Mar 03, 2011 Mar 31
COMA32	12:57:47.566	+27:59:30.49	24.5	28.4	0.7	2011 Mar 02
COMA33	12:57:48.401	+28:30:29.69	24.5	28.3	0.8	2011 Mar 02
COMA34	12:57:48.663	+29:01:43.42	24.5	28.6	0.7	2011 Apr 01
COMA41	12:55:57.916	+27:28:44.78	24.5	28.4	0.7	2011 Mar 31
COMA42	12:55:58.729	+27:59:44.24	24.5	28.3	0.7	2011 Mar 31
COMA43	12:55:59.545	+28:30:42.91	24.5	28.4	0.8	2011 Mar 31
SDF	13:24:39.758	+27:28:57.16	46.5	28.6	0.7	2008 Jun 05

Note.
[a] 1-σ of background variation in 2 arcsec apeture in units of mag arcsec^{-2}.

2. SELECTION OF UDGs

2.1. Suprime-Cam Imaging Data of the Coma Cluster

We retrieved a wide W-C-RC band (R-band) survey of the Coma cluster of Suprime-Cam from the Subaru public archive (SMOKA; Baba et al. 2002). The data used in our UDG detection is listed in Table 1. The survey field consists of 18 fields of 30 × 37 arcmin. Each field has about six arcminutes of overlap with adjacent fields. The size of the survey field is about $1°.7 \times 2°.7$ with northwest and southwest corners indented (Figure 1), which is about 15 times larger than a single field.

Most of the data were originally used by Okabe et al. (2014). They did not use all of their data, probably because good seeing is required for their analysis of weak gravitational lensing. Meanwhile, our targets are much more extended and fainter objects, and less affected by point-spread function (PSF) blur. We therefore coadded all the data. In this study, we reduced all the data with an improved procedure (e.g., with a cross-talk correction Yagi 2012). Flat images are constructed from the same data set (night sky flat). The sky background was subtracted in a 256 × 256 pixel (51.7 × 51.7 arcsec) square mesh. Since the size of the target objects in this study is expected to be smaller than 30 arcsec (∼15 kpc), the background size is large enough. The mosaicked images were constructed at each field. Background noise was estimated from a MAD (median of absolute deviation) of 10^6 random sampling of two-arcsecond aperture photometry. The values are shown in Table 1.

The flux zero point was calibrated using the Sloan Digital Sky Survey 3 (SDSS3) Ninth Data Release (DR9) catalog (Ahn et al. 2012) following the recipe in Yagi et al. (2013). We adopted the conversion from SDSS r and $r − i$ color to the Suprime-Cam R-band as

$$R - r = \sum c_k (r - i)^k \qquad (1)$$

and coefficients are given in Table 2. Since the magnitude zero point of SDSS is suggested to have a small offset from the AB magnitude system, we corrected the offset as $m_{AB} - m_{SDSS} = 0.012(g)$ and $0.010(r)$, using the values given by the "K-correct" software (Blanton & Roweis 2007) v4. About a hundred $19 < r < 21$ stars were used for the calibration in each field, and the statistical errors estimated from MAD were less than 0.03 mag.

The Galactic extinction in the R-band of the 18 fields varies between 0.016 and 0.031 mag according to NASA/IPAC Extragalactic Database (NED),[7] which is based on Schlafly & Finkbeiner (2011) and Schlegel et al. (1998). We assume that the variation of the extinction is small and negligible within each field, and used the value at the center. Hereafter, the magnitudes and the SB are after the correction of the Galactic extinction.

The celestial coordinates were calibrated with WCSTools (Mink 2002) referring to the Guide Star Catalog 2.3 (Lasker et al. 2008). The coordinates are used to cross-identify against other catalogs.

Object detection and photometric measurement was performed with SExtractor (Bertin & Arnouts 1996) version 2.19.5. The detection parameters are 27.3 mag arcsec^{-2} (after the Galactic extinction correction) and 10 pixels.

2.2. Counterpart of DF-UDG

In the catalog made by SExtractor, we first identified DF-UDGs. Our survey field covered 40 out of the 47 DF-UDGs. Except for the faintest one (DF27), DF-UDGs are easily identified with enough S/N in the image of ∼20 minutes integration by Suprime-Cam in the R-band using the coordinates given in van Dokkum et al. (2015a). They are also found in our catalog made by SExtractor. Though the
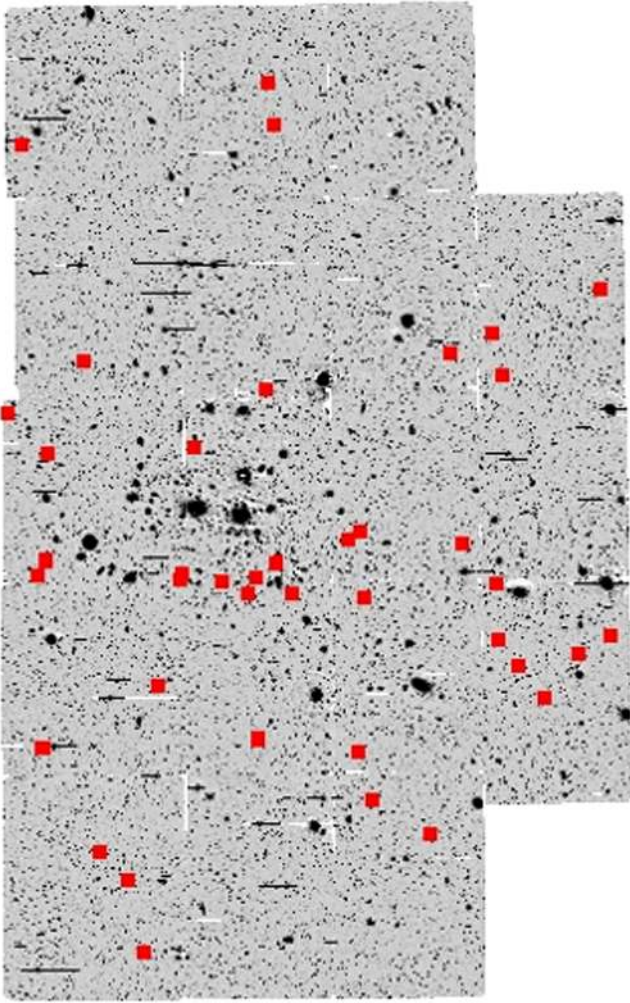
---

[7] http://ned.ipac.caltech.edu/

Figure 1. Cross-matched objects in the Suprime-Cam field with the objects in Figure 1 from van Dokkum et al. (2015a). The blue rectangles show a Dragonfly FOV (2.86 × 2.90 degrees) by van Dokkum et al. (2015a).

coordinate of DF27 in van Dokkum et al. (2015a) appears to be about 15 arcsec off from its possible UDG counterpart in the Subaru image, we include the galaxy as one of the 40 DF-UDGs.

2.3. Selection Based on SExtractor Output

We adjusted criteria to select objects that are "similar" to the 40 DF-UDGs from the photometric parameters of those detected in the Subaru data. We also aim to find fainter and/or more extended ones if they exist.

After some trials, we adopted the following selection criteria:

1. SExtractor's FLAGS is smaller than 4. Deblend and nearby bright object are permitted, but objects with other defects are rejected.
2. The Petrosian radius is measured (not zero).
3. The R-band magnitude (R) is between 18 and 26 mag, which corresponds to $-17 < M_R < -9$ at the Coma cluster.
4. The FWHM is larger than four arcseconds (~1.9 kpc at the Coma cluster).

5. The half light radius is larger than 1.5 arcsec (~0.7 kpc). As several half light radii are used in this study, we call this SExtractor output $r_{e,S}$ hereafter.
6. The mean SB within $r < r_e$ is between 24 and 27 mag arcsec^{-2} in R-band. The mean SB is referred to as $\langle \mu(r_e) \rangle$ hereafter.
7. The difference between $\langle \mu(r_e) \rangle$ and the local SB at $r_{e,S}$ ($\mu_{e,S}$ hereafter) is smaller than 0.8 mag arcsec^{-2}.

The SExtractor output parameters used in this study are described in Appendix A. The criteria are applied sequentially. The number of objects after the application of each criterion is shown in Table 3.

Criteria 1 and 2 help remove false detections. The bright-end limit of criterion 3 works as a dwarf selection, which is $M_R \gtrsim -17$ at the Coma cluster. The faint-end limit ($R < 26$) removes noisy detection. As the detection threshold we adopted was 27.3 mag arcsec^{-2}, the area of 26 mag object is smaller than a $r = 1$ arcsec circle. Such faint and compact objects are also rejected by the criteria.

Criterion 4, FWHM selection, is the strongest selection criterion. It makes the number of samples about $1/100$ ($1,240,262 \rightarrow 12,389$), and it is the primary criterion for the galaxy size. Van Dokkum et al. (2015a) defined UDG as $r_e \gtrsim 1.5$ kpc and $\mu_0 \gtrsim 24$ g mag arcsec^{-2}. These parameters are obtained from GALFIT (Peng et al. 2002, 2010) using an exponential profile,

$$I = I_0 \exp(-\alpha r / r_e), \tag{2}$$

where I is the SB at the radius of r, I_0 is the central SB, and $\alpha \simeq 1.6783$ is a scaling parameter so that the flux within $r < r_e$ is half of the total flux. As discussed later, some parameters from SExtractor and GALFIT (e.g., effective radius) turned out to be not always consistent. Moreover, GALFIT did not converge for some galaxies. We therefore use the parameters from SExtractor for the sample selection, and obtain additional parameters using GALFIT later.

Since our sample at this stage is large ($>10^6$), we cannot practically run GALFIT before some kind of screening. We compared FWHM and the effective radius of SExtractor output ($r_{e,S}$) and decided to use FWHM primarily.

As shown in Figure 2, $r_{e,S}$ shows a systematic trend with R-band magnitude that brighter objects tend to have larger $r_{e,S}$. On the other hand, such a trend is not seen in FWHM (Figure 3). Though it is uncertain whether the trend is intrinsic or artificial, we adopted FWHM as the primary criteria in this study, we used $r_{e,S}$ supplementarily in criterion 5. Since the FWHM of SExtractor is calculated from Gaussian fitting, the r_e criterion by van Dokkum et al. (2015a) cannot be converted analytically. We set the FWHM criterion so that all 40 DF-UDGs satisfy FWHM > 4 arcsec in our catalog (Figure 3).

At the Coma distance, $r_e \gtrsim 1.5$ kpc corresponds to $r_e \gtrsim 3.2$ arcsec. However, 8 of the 40 DF-UDGs do not satisfy $r_{e,S} \gtrsim 3.2$ arcsec. Moreover, we found that there are some extended objects with smaller $r_{e,S}$ than the UDGs of van Dokkum et al. (2015a). We therefore adopted the criterion $r_{e,S} > 1.5$ arcsec, which is roughly comparable to the FWHM > 4 arcsec criterion (Figure 4).

In the exponential profile, the local SB at $r = r_e$ (μ_e) and the mean SB within $r < r_e$ ($\langle \mu(r_e) \rangle$) can be converted from μ_0 as

$$\mu_e \simeq \mu_0 + 1.822, \tag{3}$$

Table 2
The Coefficients of Color Conversion

SDSS-Suprime	CCD	SDSS	Range	c_0	c_1	c_2	c_3	c_4	c_5	c_6	c_7
$r - R$	HPK	$r - i$	$-0.6 < r{-}i < 0.6$	0.006	0.312	-0.064	-0.152	1.601	-1.262	-7.990	9.992

and

$$\langle \mu(r_e) \rangle \simeq \mu_0 + 1.124. \tag{4}$$

As the color of most galaxies in the Coma cluster is expected to be $g - R \sim 0.5 \pm 0.5$, we adopt the criterion $\langle \mu(r_{e,S}) \rangle > 24$ for our R-band data. We also set a fainter threshold, $\langle \mu(r_{e,S}) \rangle < 27$, so that spurious detections would be rejected (Figure 5).

Criterion 7 requires that $\Delta\mu = \mu_{e,S} - \langle \mu(r_{e,S}) \rangle < 0.8$. It helps remove close overlap of compact objects. If we assume a pure Sérsic profile (Sérsic 1968),

$$I = I_0 \exp \left\{ -\alpha_n \left(\frac{r}{r_e} \right)^{\frac{1}{n}} \right\}, \tag{5}$$

for the objects, this criterion corresponds to $n \lesssim 1.25$. α_n is calculated by solving

$$\Gamma(2n) = 2\gamma(2n, \alpha_n), \tag{6}$$

where $\Gamma()$ and $\gamma()$ are the Gamma function and incomplete gamma function, respectively (Graham & Driver 2005). The Sérsic profile with $n = 1$ is a pure exponential profile, and the profile is adopted by van Dokkum et al. (2015a) for DF-UDGs. The distribution of $\Delta\mu$ and the border of the criterion are shown in Figure 6.

We thus adjusted the seven objective criteria based on the SExtractor outputs so that all the DF-UDGs are included in our Subaru-UDG catalog and that other brighter and/or more compact galaxies are removed as much as possible. The galaxies that passed the criteria are therefore expected to be similar to the DF-UDGs.

2.4. Eyeball Inspection

After the screening by the seven criteria, several artifacts and non-UDG objects are still contaminated. We made postage stamps 40×40 arcsec in size for eyeball inspection. All four authors classified the candidates independently, and chose a score: a candidate(1), uncertain(0.5), or not a candidate(0). We used the postage stamps of the 40 DF-UDGs in the Subaru image as a fiducial set, and removed other kinds of objects. If the total score was three or more (the full score was four), it was cataloged. This means that at least two of us classified an object as a candidate, and the other two were uncertain or one of the two classified the object as a candidate.

The rejected objects include non-UDG objects (e.g., a tidal tail, part of a spiral arm, blended compact objects, etc.), debris of cosmic rays and moving objects, and artifacts (e.g., ghosts of optics, blooming, CCD defect, edge of the field, etc.). In some cases, a UDG has more than one peak. These are merged into one entry. We also noticed that the debris of a bright moving object mimics a UDG after coadding the exposures. These contaminants are removed manually. After removing such redundancy, 854 objects remain. We call the 854 objects Subaru-UDGs in the Coma cluster (Table 4).

2.5. Control Field

We retrieved the R-band data of the Subaru Deep Field (SDF; Kashikawa et al. 2004) taken on 2008 June 05 (UTC) for a control field. It covers a single 30×37 arcmin field. The coadd of 5×480 s and 390.4 s (cloudy) is made in the same way as the Coma cluster fields. The 1-σ of background variation in the two-arcsecond aperture is 28.6 mag arcsec^{-2}, which is comparable to the Coma fields. We searched for UDGs in the same way as in the Coma fields. As shown in Table 3, 13 objects satisfied the seven criteria of the SExtractor parameters, and our eyeball inspection rejected all 13.

3. PROFILE PARAMETERS OF SUBARU-UDGS

We derived a profile parameter of Subaru-UDGs using GALFIT (Peng et al. 2002, 2010), and examined the errors and the consistency.

3.1. Fitting with GALFIT

We used GALFIT version 3.0.5 (Peng et al. 2010) for fitting the Sérsic profile (Sérsic 1968) to the Subaru-UDGs. We started with extracted 40×40 arcsec postage stamps that were used for eyeball inspection. As the target object is often blended with other objects, we applied a mask using a SExtractor's segmentation image. The fit was performed in a cutout of $2 \times$ FWHM square around the detected center from the SExtractor. If the size is larger than the postage stamp size, the whole postage stamp is used. The PSF is made in each field using 20–70 stars. The PSF selection criteria we adopted are CLASS_STAR > 0.8, FLUX_MAX is not saturated and not too small, FLAG $= 0$, and axis ratio $b/a > 0.95$. In Figures 7 and 8, we show several examples.

In some cases, the fitting did not give a reasonable result. And we realized that r_e from GALFIT is often larger than that from SExtractor ($r_{e,S}$), and is sometimes unreasonably large. We therefore set two criteria for accepting the fitting result:

1. reduced χ^2 of the fitting satisfies $\chi^2_\nu < 1$, and
2. $r_e \leqslant 3 \times r_{e,S}$.

From 854 Subaru-UDGs, 83 were rejected by criterion 1, and 18 were rejected by criterion 2. The difference of the number from Koda et al. (2015) is due to no manual masking.

One reason why GALFIT did not converge is a contamination of the outskirts of the neighboring large galaxy, since we fixed the background to be 0 in the fitting. Another reason is that some objects show a compact nucleus-like feature, which resembles dE,Ns (Binggeli et al. 1984). This kind of object is investigated later (Section 3.3).

The catalog of the best-fit parameters of good fitting results are given in Table 4 (the full catalog is available in the online journal as a machine-readable table). The magnitude, r_e, Sérsic n, axis ratio, and position angle (PA) were taken from the output of GALFIT. The PA is converted so that PA is zero when the major axis aligns in the north–south direction and increases counterclockwise, e.g., the NE–SW major axis is positive PA. The central SB (μ_0) was converted from the

Table 3
Number of UDG Candidates after Applying Criteria

Field	All	1	2	3	4	5	6	7	Eye
coma10	156,187	146,305	131,192	63,584	805	168	99	66	27
coma11	178,088	169,078	155,263	71,236	541	240	145	100	68
coma12	192,439	176,787	160,192	71,532	699	358	212	154	113
coma13	160,376	155,035	146,728	69,302	418	174	84	50	31
coma14	165,194	160,564	151,905	74,932	519	184	102	45	15
coma20	145,652	138,543	129,955	65,506	554	204	87	44	23
coma21	137,817	133,248	128,073	69,544	646	370	194	120	79
coma22	202,816	184,165	162,652	70,526	1479	665	383	288	177
coma23	187,945	164,277	146,051	62,727	690	277	159	105	51
coma24	164,345	158,799	150,913	68,862	354	131	69	39	20
coma30	170,689	161,551	151,340	71,642	564	230	115	72	36
coma31	177,948	159,296	150,457	73,014	603	285	167	113	85
coma32	158,493	150,294	139,264	67,823	826	338	207	158	124
coma33	211,276	183,982	156,273	63,350	1070	252	162	124	55
coma34	196,346	183,057	166,032	73,852	412	121	66	36	22
coma41	150,547	144,179	133,967	65,099	690	270	163	102	60
coma42	176,925	167,041	150,546	68,795	871	339	174	124	71
coma43	194,139	179,433	158,850	68,936	648	135	73	39	25
Total	3,127,222	2,915,634	2,669,653	1,240,262	12,389	4741	2661	1779	1082
SDF	198,392	182,111	166,412	72,265	358	71	29	13	0
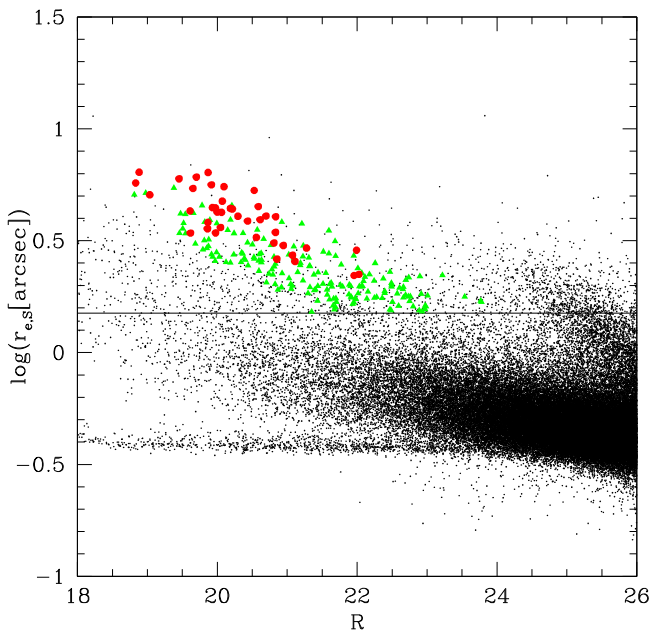
Figure 2. Magnitude–log($r_{e,s}$) diagram. The dots represent objects of the COMA22 field after the application of criteria 1–3. The abscissa shows R-band Kron magnitude after the Galactic extinction correction, and the ordinate is the log of $r_{e,S}$ in arcseconds. DF-UDGs are overplotted as red filled circles. The horizontal solid line corresponds to criterion 5; $r_{e,s} > 1.5$ arcsec. The Subaru-UDGs in the COMA22 field are shown as green filled triangles.

Figure 3. Same as Figure 2 but the ordinate is the log of the FWHM in arcseconds. Criterion 4, FWHM > 4 arcsec, is shown as a horizontal solid line.

central pixel value of the model FITS image. Following Koda et al. (2015), we will call the objects with $r_e > 1.5$ kpc MW-sized Subaru-UDGs. Among the 753 objects that have any good fitting result, 322 satisfy the criterion.

3.2. Consistency among Multiple Measurements

The stability of the fit parameters is examined using objects in overlapping regions of fields. We compared 250 pairs of good fitting results of the same object in different fields. The
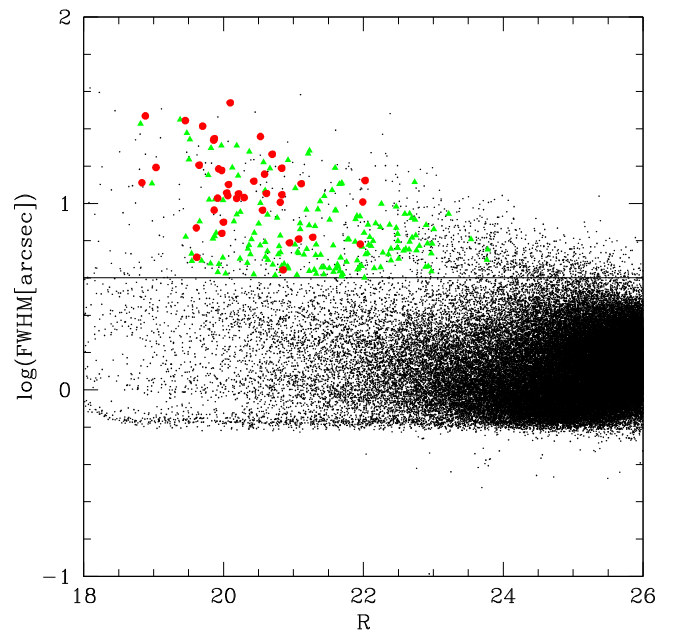
results are shown in Figure 9. The fitting results show much larger dispersion than calculated from GALFIT. Figure 10 shows the GALFIT-based error and the dispersion of the magnitude. The error of the parameters are estimated as $1/\sqrt{2}$ of MAD-based rms of the difference. They are 0.08 mag, 0.07, and 0.02 for magnitude, Sérsic n, and b/a, respectively, and 0.06 dex for the relative error of r_e. The errors are significantly larger than the ones that GALFIT reports on each single image, which are given in Table 4. It implies that the S/N of these objects obtained from ~30 minutes exposure with the 8 m telescope is still insufficient for the profile fitting of
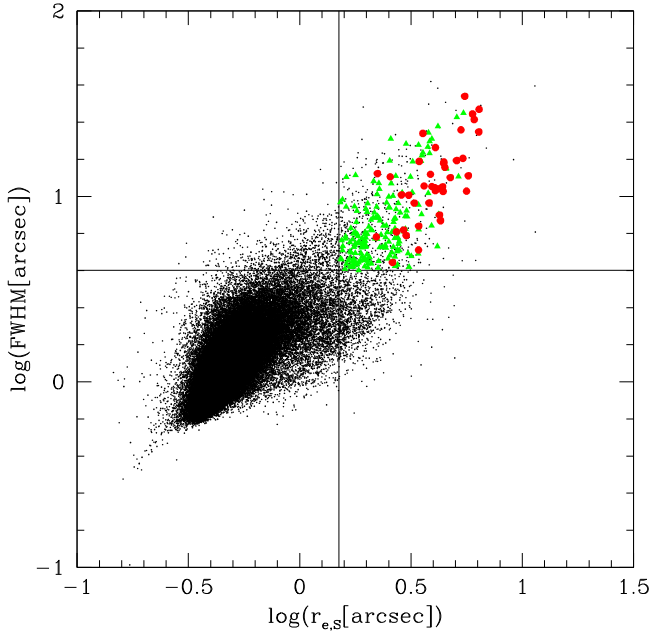
Figure 4. $\log(r_{e,S})$ vs. $\log(\mathrm{FWHM})$ diagram of COMA22 objects after application of criteria 1–3. DF-UDGs are overplotted as red filled circles. The Subaru-UDGs in COMA22 field are shown as green filled triangles. The horizontal line shows criterion 4 and the vertical line shows criterion 5.
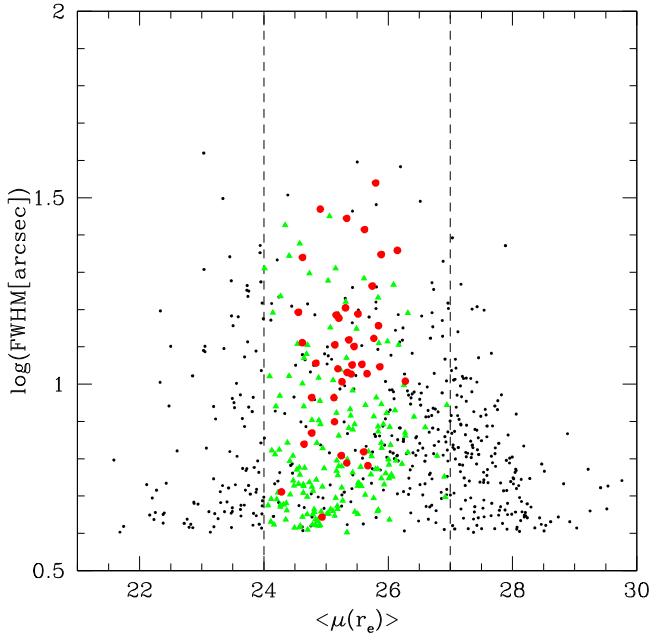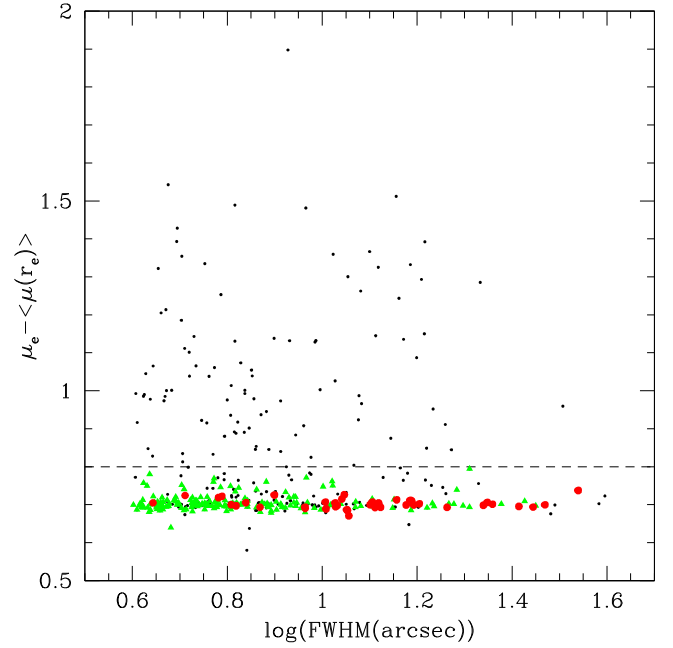

Figure 6. $\log(\mathrm{FWHM})$ vs. $\Delta\mu$ diagram. The dots represent objects of the COMA22 field after application of criteria 1–6, and DF-UDGs are overplotted as red filled circles. The Subaru-UDGs in the COMA22 field are shown as green filled triangles. The broken line shows criteria 7.

component model. Two criteria are the same as those for the one-component model, and an additional one is that the PSF position should be within two arcseconds from the Sérsic center. We obtained a fitting result for 693 UDGs, while others did not converge, possibly because the Sérsic profile alone can make a good fit. Forty-eight are rejected by the $\chi_\nu^2 < 1$ criterion, six are rejected by the $r_e \leqslant 3 \times r_{e,S}$ criterion, and thirty are rejected because PSF and Sérsic components are separated by > 2 arcsec. Finally 609 remain as good PSF +Sérsic fits. Their parameters are given in Table 4.

In some cases the two-component model fit better than the single Sérsic model, while in other cases the two-component model does not fit at all. For an objective selection of the better model, we adopted a Bayesian information criterion (BIC)

$$\mathrm{BIC} = N\ln(\chi^2/N) + \mathrm{npar}\ln(N), \qquad (7)$$

where $N = \mathrm{ndof} + \mathrm{npar}$, and ndof is a degree of freedom in GALFIT. npar $= 7$ for the Sérsic single model and npar $= 10$ for the PSF+Sérsic model. Only 163 UDGs show that Sérsic single model is better, and the PSF+Sérsic model is better for the other 446. Whether the PSF+Sérsic model is better or not is given in the last column of Table 4.

The r_e of the one-component fitting and the two-component fitting is consistent in most cases (Figure 11). Especially those objects for which the Sérsic single model is fitted better show good agreement of r_e in the two models. The Sérsic n versus the ratio of r_e plot (Figure 11) shows that in the case where the PSF+Sérsic fit works better the results from the Sérsic single model fit tend to show large n and r_e. It would be the effect of the central nucleus that mimics a large n profile at the center.

If we used r_e from the PSF+Sérsic model when the fitting is better (with smaller BIC), the number of MW-sized Subaru-UDGs ($r_e > 1.5$ kpc) is 328. Some galaxies that were rejected by the $r_e \leqslant 3 \times r_{e,S}$ criterion were recovered by the PSF +Sérsic fitting, and the number is slightly increased.

Figure 5. $\log(\mathrm{FWHM})$ vs. mean surface brightness ($\langle\mu(r_{e,S})\rangle$) diagram. The dots represent objects of the COMA22 field after the application of criteria 1–5, and DF-UDGs are overplotted as red filled circles. The Subaru-UDGs in COMA22 field are shown as green filled triangles. Vertical broken lines show criterion 6.

UDGs. Meanwhile, the error of the parameters does not severely affect the following analysis.

3.3. Comparison of One-component and Two-component Models

For checking the possible nucleus in UDGs, we tried to fit the PSF+Sérsic two-component model for all of the Subaru-UDGs. We set three criteria for accepting the fit of the two-

Table 4
SC-UDG Catalog

SC-UDG ID	R.A.(J2000)	Decl.(J2000)	R[a]	$B - R$[b]	Other Catalogs[c]	Spectroscopy[d]
1	13:00:17.087	+27:03:04.12	…	…	…	…
2	13:00:25.342	+27:11:03.90	…	…	…	…

		SExtractor Result		
Rmag	FWHM (arcsec)	$r_{e,S}$ (arcsec)	$\langle \mu(r_{e,S}) \rangle$(model) (mag arcsec^{-2})	$\mu_{e,S}$(model) (mag arcsec^{-2})
21.4	8.7	2.5	25.7	24.6
21.7	4.1	1.7	24.8	23.8

Fit Size			Sérsic Fitting Result			
(arcsec)	mag(model)	r_e (kpc)	Sérsic n	Axis Ratio	PA (deg)	μ_0(model) (mag arcsec^{-2})
18.0	21.23 ± 0.01	1.68 ± 0.02	0.61 ± 0.02	0.68 ± 0.01	55.6 ± 1.5	25.13
8.7	21.79 ± 0.01	0.93 ± 0.01	0.77 ± 0.02	0.52 ± 0.01	39.0 ± 0.6	24.25

		Sérsic+PSF Fitting Result				Better Model[e]
mag(Sérsic)	r_e (kpc)	Sérsic n	Axis Ratio	PA (deg)	mag(PSF)	
21.19 ± 0.01	1.84 ± 0.01	0.70 ± 0.01	0.64 ± 0.00	50.3 ± 0.6	27.03 ± 0.16	2
21.81 ± 0.01	0.94 ± 0.01	0.75 ± 0.02	0.51 ± 0.00	38.8 ± 0.5	26.75 ± 0.31	1

Notes.
[a] R-band(AB) Kron magnitude from Yamanoi et al. (2012).
[b] $B - R$(AB) color in 2″ aperture from Yamanoi et al. (2012).
[c] DF (van Dokkum et al. 2015a), GMP (Godwin et al. 1983), IBG (Iglesias-Páramo et al. 2003), APS (Adami et al. 2006a), ASU (Adami et al. 2006b), HdBVK (Hoyos et al. 2011), YKK (Yamanoi et al. 2012, unpublished).
[d] Spectroscopic confirmation.
[e] 1: Sérsic single model is better; 2: PSF+Sérsic model is better; 0: GALFIT failed.

(This table is available in its entirety in machine-readable form.)

3.4. Eyeball Inspection Rejected Objects

We also tried to apply GALFIT to objects that were rejected by eyeball inspection. A total of 672 postage stamps were marked as non-UDGs (score < 3.0). GALFIT failed to fit 179 of them, and 244 has $\chi^2_\nu \geqslant 1$. The remaining 249 rejected objects and 768 UDGs are plotted on the $\log(r_e)$ versus log (Sérsic n) plane as the left panels of Figure 12. In the right panels of Figure 12, the mean SB in r_e ($\langle \mu(r_e) \rangle$) versus $\log(n)$ plots are shown. We derived $\langle \mu(r_e) \rangle$ from the GALFIT result as

$$\langle \mu(r_e) \rangle = \text{mag} + 5 \log(2\pi r_e^2 (b/a)). \quad (8)$$

From the figures, some rejected objects have parameters similar to the UDGs, while some have quite different parameters. One of the deviated groups is the small n, moderate r_e, and $\langle \mu(r_e) \rangle$ one. Most such objects have a score = 0, e.g., an edge of the ghost, a tidal tail, and a blend of compact objects with the outskirts of a larger galaxy. Another deviated group is the large n, r_e, and $\langle \mu(r_e) \rangle$ one, which is seen in any score; e.g., probable background spiral, a blended object, and a compact object. And examples of objects with similar parameters to the UDGs are background edge-on galaxy, edge of ghost, and low S/N features, possibly tidal debris. The result shows that the GALFIT parameters may help us in the effective rejection of non-UDG contaminants from the list in the SExtractor-based selection, but the selection is still not perfect and several types of objects contaminate.

3.5. Comparison of DF-UDGs and Subaru-UDGs

Figure 13 shows the distribution of Subaru-UDGs and DF-UDGs measured in our Subaru data in GALFIT parameter space. Van Dokkum et al. (2015a) adopted a pure exponential disk fitting ($n = 1$ fixed), while we set n as a free parameter. The data used by van Dokkum et al. (2015a) are in the i-band, while the data in this study are in the R-band. Even though these differences exist, their criterion of $r_e \gtrsim 1.5$ kpc was reproduced for DF-UDGs in our measurement. The $\log(r_e)$ versus $\log(n)$ plot shows that Subaru-UDGs includes more compact objects than DF-UDGs. In the $\langle \mu(r_e) \rangle$ versus $\log(n)$ plot, the Subaru-UDGs and DF-UDGs show comparable distribution. In the right panel of Figure 13, MW-sized Subaru-UDGs are compared with DF-UDGs. Though some Subaru-UDGs have higher and lower mean SB, the distribution is still comparable.

4. PROPERTIES OF SUBARU-UDGs

In Koda et al. (2015), we analyzed the internal structures of the UDGs. On average they have relatively smooth light distributions with exponential profiles. They follow the red sequence of the Coma cluster members and thus are a passively evolving galaxy population. In this section, we investigate their distributions within the cluster and compare the nucleated UDGs with other nucleated dwarf populations.
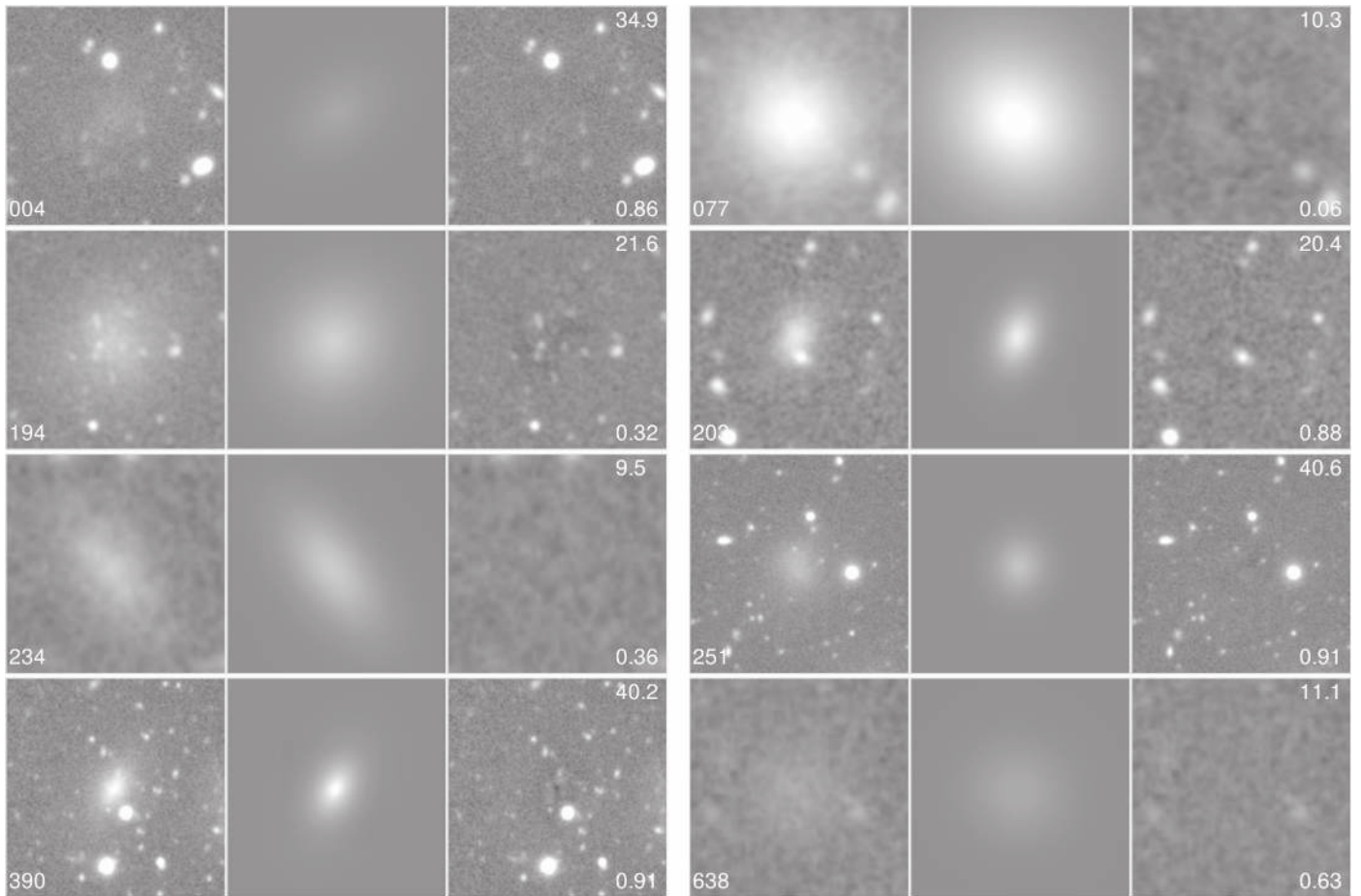
Figure 7. Examples of one-component fitting to UDGs. From the left, the original cutout, GALFIT model, and the residual image after the model subtraction are shown. One count corresponds to 33 mag pix^{-1} ~ 29.5 mag arcsec^{-2}, and the scale of the image is from −50 count to 200 counts. The ID of Table 4 is shown at the bottom left. The size of the cutout is shown at top right in an arcsecond scale, and the reduced χ^2 of the fitting is shown at bottom right.

4.1. Radial Distribution

The radial profile of the surface number density of Subaru-UDGs (logarithmic scale) is shown in Figure 14 as a function of the projected distance to the cluster center. Following Koda et al. (2015), we adopted (R.A., Decl.)(J2000.) = ($12^h59^m42^s.8$, $+27°58'14''$) (White et al. 1993) as the center of the Coma cluster. In each annulus, the area is calculated considering the coverage of the observed area. The error bars show Poisson error.

We also plotted the surface number density profile of giant Coma cluster member galaxies from SDSS DR7 (Abazajian et al. 2009) selected by $r < 16$ mag and $0.015 < z < 0.030$. The ordinate is shifted by $+0.5$ dex for comparison. We assumed that the spectroscopic target selection of SDSS is unbiased and uniform. In the plot, the possible incompleteness of SDSS spectroscopy (~10%; Adelman-McCarthy et al. 2007)[8] is not corrected.

The general trends of the two profiles are similar, and their slopes are comparable. At the very center, the number of Subaru-UDGs appear slightly lower than that of giants. This could be due to an incompleteness detection of UDGs due to confusion as suggested by van Dokkum et al. (2015a) and Koda et al. (2015). The two profiles do not match within the error bars in $0°.6–1°.0$ (1.0–1.7 Mpc in projected distance), and

there is a possible excess of Subaru-UDGs relative to the giants. It is not clear if this excess is real or due to some selection bias.

Structural parameters are plotted against the cluster-centric distance in Figure 15. There are several potential selection biases due to our detection and selection criteria, including the eyeball selection. These could introduce artificial radial gradients or blur them. For example, the central region is much more crowded and it is more likely to miss some UDGs in detection, especially the ones with lower SBs and more extended sizes. The effect of confusion would be higher for low SB and much extended ones. In parametric selection, UDGs are selected by SB and size in nature. We adopted $\langle \mu(r_{e,S}) \rangle - \mu_{e,S} < 0.8$, which set a constraint on Sérsic n, which reflects the luminosity concentration. These selection criteria may affect the range of μ_e and b/a, and possibly their radial trends. In addition, these potential biases, e.g., on μ_e and b/a, can be carried to other parameters as they are often correlated. In Figure 15, the structural parameters of the UDGs in this paper do not show any clear radial trend. A detailed examination of potential biases is beyond the scope of this paper and should be given in a future study.

4.2. Radial Alignment of UDGs

The measurement of PA should not be biased by our detection and selection criteria as discussed in the previous

---

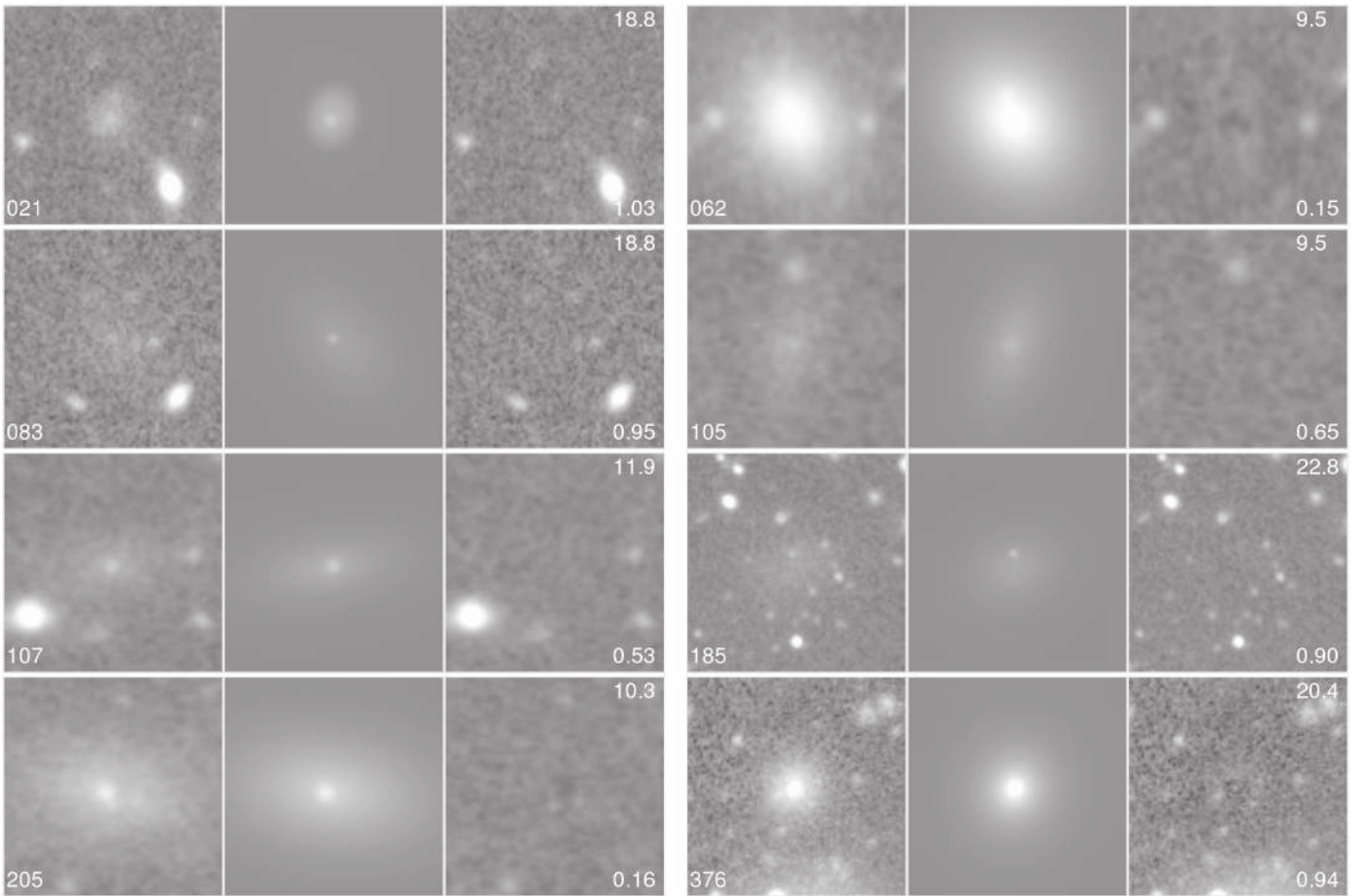[8] http://classic.sdss.org/dr7/products/spectra/special.html

Figure 8. Same as Figure 7, but of the two-component fitting to UDGs.

section. It is interesting that we found that the major axes of the Subaru-UDGs are preferentially oriented toward the cluster center.

The PAs measured from the direction toward the cluster center (φ) are shown as a histogram in Figure 16. In the plot, we removed round UDGs with $b/a \geqslant 0.85$ since their PA measurements should have large error. The plot includes 564 UDGs after the b/a selection. The figure suggests that UDGs are preferentially elongated along the radial direction ($\varphi \sim 0$). As a simple statistical test, we compared the numbers of radially elongated ($\varphi < 45$) UDGs and azimuthally elongated ($\varphi \geqslant 45$) ones (two-bin test; cf. Thompson 1976; note that Thompson 1976 applied a χ^2 test, while we calculated the p-value using the binomial distribution). If the orientation is random, the two numbers should be comparable and follow a binomial distribution $B(564,0.5)$. However, there are 322 radially elongated UDGs and 242 azimuthally elongated ones, and the hypothesis that the orientation is random is rejected with a p-value $\sim 0.04\%$.

This preferred orientation has a radial dependence as a function of the projected distance from the cluster center. We divide the sample into three according to the projected distance from the cluster center at 1500 and 2700 arcsec so that the sample sizes of the three are comparable. The result is shown in Figure 17. The preferred orientation toward the cluster center is the most significant in $d < 1500$ arcsec (the bottom panel), while this trend decreases in $1500 < d < 2700$ arcsec (middle). The distribution appears nearly random in $d > 2700$ arcsec.

The two-bin test of the radial/azimuthal comparison shows that $d < 1500$ arcsec and $1500 < d < 2700$ arcsec has a p-value $\lesssim 0.4\%$. It means that the preference of radial alignment is statistically significant. In $d > 2700$ arcsec, the number of radial and azimuthal ones are the same. The same trend is seen if we limit the sample in MW-sized UDGs. For comparison, we also analyzed the bright ($r < 18$) cluster members in SDSS DR7 used in previous sections and we confirmed that the radial alignment does not exist in the bright members.

4.3. Nucleated Dwarfs

In Section 3.3, we tried PSF+Sérsic fitting. If we define nucleated UDGs as those that obtained a better fit with the Sérsic+PSF model than with the Sérsic alone model, a large fraction of Subaru-UDGs are nucleated and the nucleated UDGs show a similar trend to the other nucleated populations.

The nucleation fraction (f_N) of UDGs is $>52\%$, and the f_N of MW-sized UDGs is $>62\%$. As described in Section 3, some of the UDGs were not fitted well with either model, and therefore it is uncertain whether they are nucleated or not. Figure 18 shows f_N as a function of the absolute magnitude. We also checked that there is no significant trend in f_N along the distance from the center.

The high f_N is suggested by previous studies (e.g., Graham & Guzmán 2003; Côté et al. 2006; den Brok et al. 2014). Den Brok et al. (2014) showed that f_N gradually becomes lower as the magnitude becomes fainter. In their Figure 4, f_N is between
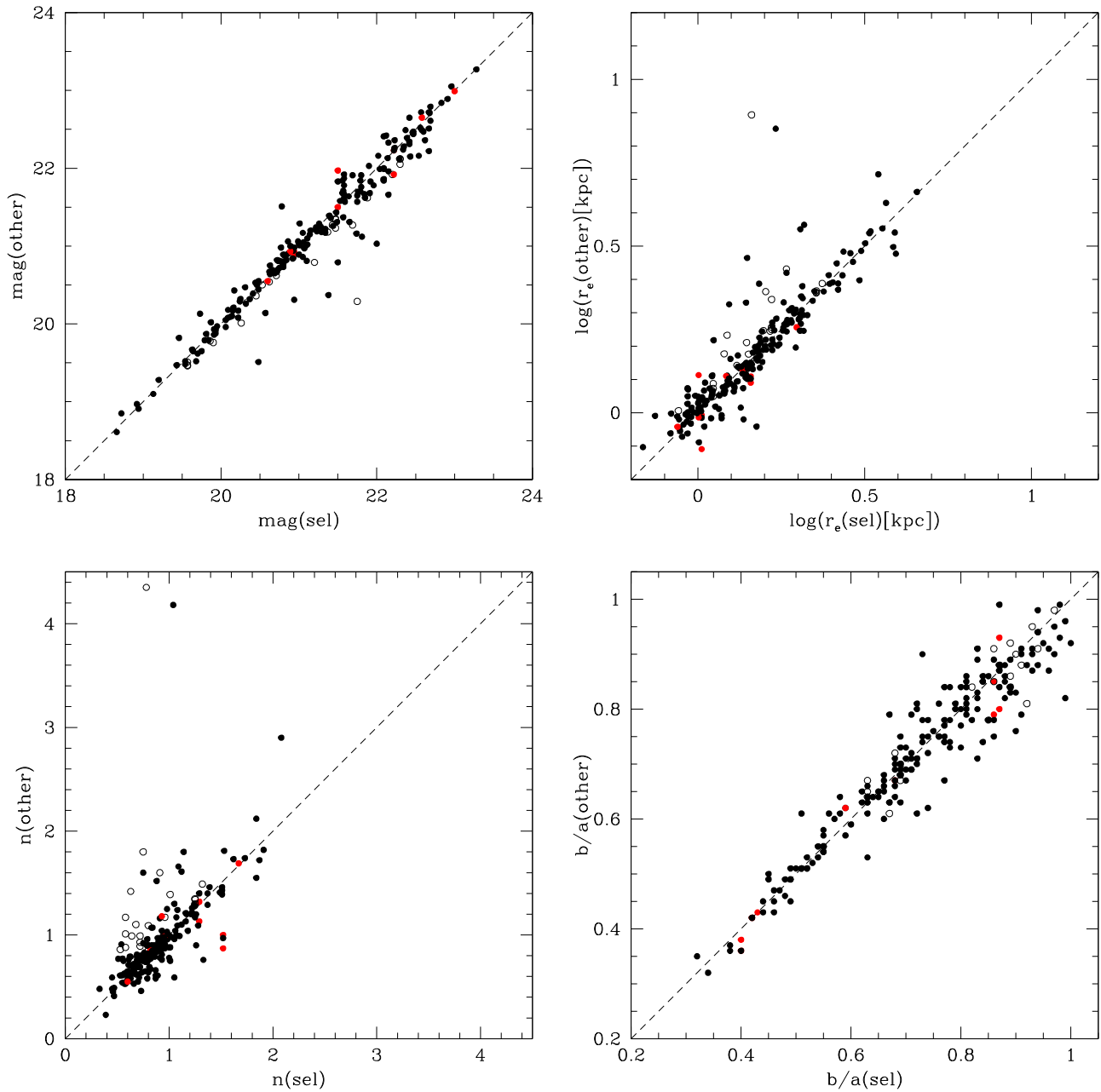
Figure 9. Comparison of fitted parameters in overlapped regions. Open circles are nucleated objects. Red filled circles have a score <3 according to our eyeball inspection. The parameters of the selected postage stamp given in Table 4 are shown on the abscissa, and those of the other postage stamp are shown on the ordinate. The comparison is shown of magnitude (top left), $\log(r_e)$ (top right), Sérsic n (bottom left), and b/a (bottom right).

0.5 and 0.8 in $-13 < M < -16$ F814W mag. Recently, Muñoz et al. (2015) measured the f_N of Fornax UDGs based on ground-based observation. They reported $f_N > 75\%$ at $M_i \simeq -15$, while $f_N \simeq 3\%$ at $M_i \simeq -11$. These results are comparable to our result except for the faintest end. Our study might have missed the nucleus of some UDGs due to blurring by a larger PSF size of the ground-based telescope for the Coma cluster. As the distance to the Fornax cluster is about one-fifth of that to the Coma cluster, faint nuclei would be more easily detected even with a ground-based telescope.

Figure 19 compares the magnitudes of the Sérsic component versus PSF for the Subaru-UDGs and the results from the *Hubble Space Telescope* (*HST*; Graham & Guzmán 2003). The blue circles show MW-sized UDGs, and the black dots are smaller ones. The green stars and broken line show the data and fit of dE,Ns in the Coma cluster, respectively, derived in the F606W band by Graham & Guzmán (2003). The nucleated Subaru-UDGs are on the correlation. The result suggests that the nuclei of UDGs are similar to those in other galaxies.

5. CROSS IDENTIFICATION WITH PREVIOUS CATALOGS OF THE COMA CLUSTER

The Coma cluster is one of the best-studied clusters of galaxies, and there are a number of galaxy catalogs in the literature. We surveyed the catalogs and identified some of the DF-UDGs and Subaru-UDGs were included (e.g., Godwin et al. 1983; Ulmer et al. 1996; Iglesias-Páramo et al. 2003; Adami et al. 2006a; Hoyos et al. 2011). In most cases the
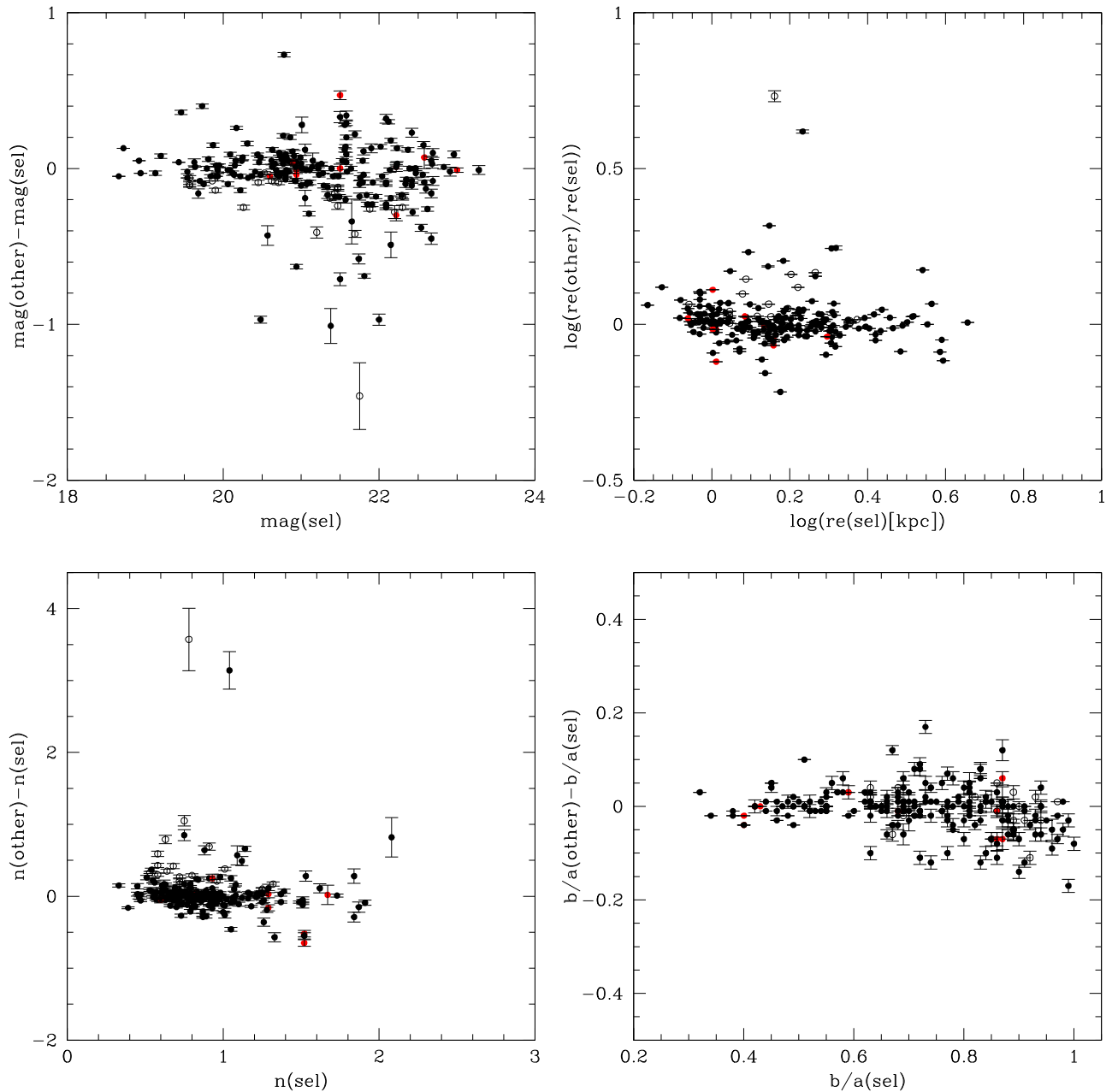
Figure 10. Comparison of fitted magnitudes. This figure is the same as Figure 9, but the ordinate is the difference of the two fittings. The error bar shows the GALFIT fitting error. The difference between two different fields is much larger than the fitting error.

central, brightest parts of UDGs were detected and cataloged, but their faint extended tail would not have always been recognized, and these galaxies did not draw a special attention until van Dokkum et al. (2015a) shed light on them. The results of our cross identification are given below. It should be noted that the previous catalogs detected the galaxies, but did not always measure their size and brightness. Therefore, they were not recognized as ultra-diffuse objects.

5.1. Optical Photometric Catalogs

5.1.1. Godwin et al. (1983)

Godwin et al. (1983) made a catalog of 6724 galaxies in the Coma cluster field in b and r bands. We cross-identified counterparts of each Subaru-UDG within 20 arcsec. In some cases, a coordinate offset, a misidentification, and/or a confusion of neighbor objects are found, and hence we make identification manually by plotting the catalog coordinate on the Subaru image and perform an eyeball inspection. Twenty-four Subaru-UDGs have counterparts in Godwin et al. (1983, GMP). The identification is given in Table 4. The overlap of DF-UDGs and GMP is only one; DF26 would be GMP2748.

Michard & Andreon (2008) gives morphological classification of 1154 GMP galaxies. In their catalog, nine Subaru-UDGs are found. Michard & Andreon (2008) classified the nine objects as five Ims, two far spirals, a dE, and a star. The classifications of faint objects are often tricky due to the low S/N. For example, our deep Subaru image shows that the object classified as a star by Michard & Andreon (2008), GMP3875, is indeed a nucleated galaxy, Subaru-UDG 335.

11
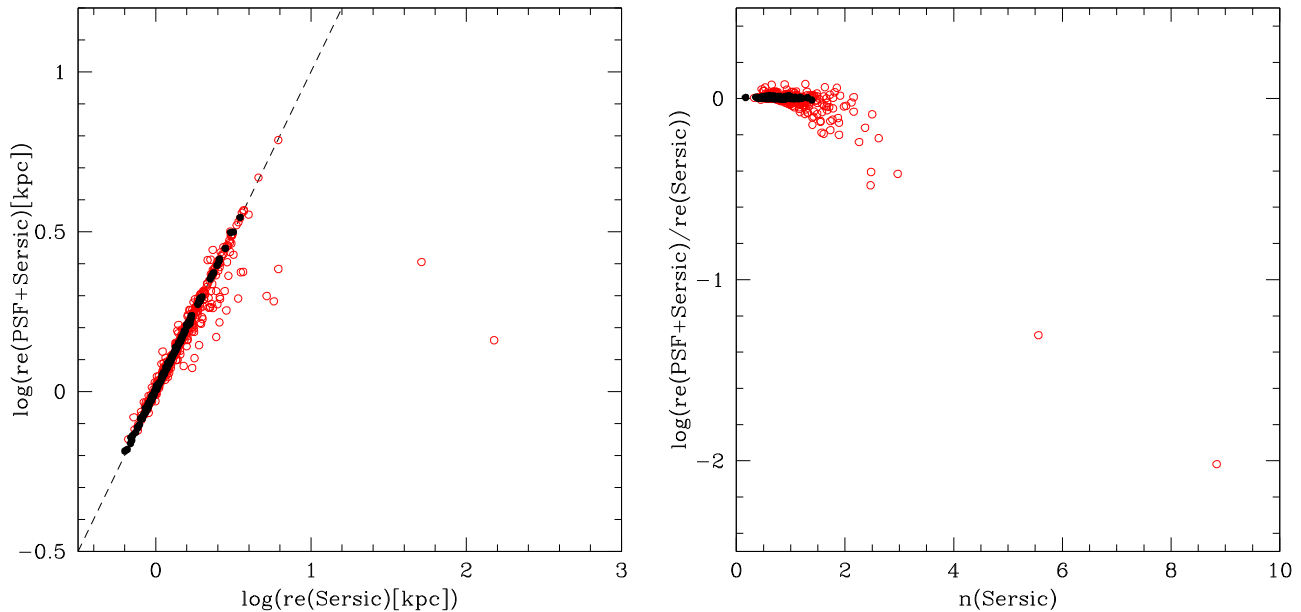
Figure 11. Comparison of Sérsic fit and PSF+Sérsic fit. Left: comparison of $\log(r_e)$ of the two models. Red open circles and black dots show those which are fitted better by the PSF+Sérsic model and the Sérsic model, respectively. Right: Sérsic n of the Sérsic fit vs. the log of the ratio of the two r_es.

We think that there are some uncertainties in their classification especially near the faint end.

5.1.2. Ulmer et al. (1996)

Ulmer et al. (1996) presented a catalog of 36 LSBs at the central region of the Coma cluster. Four Subaru-UDGs are found in the catalog (8L, 10, 11, and 18). Two of the LSBs (6, 11L) are not detected in our image, because of heavy contamination from a nearby bright galaxy. We checked the remaining 30 LSBs and find that 22 of them are removed from our catalog by the FWHM criterion (FWHM $> 4''$). Six are removed by the $r_{e,S} \geqslant 1\overset{''}{.}5$ criterion. And the $\Delta\mu$ criterion and the eyeball inspection removed one each.

Several LSBs, especially irregular ones, are deblended to portions of the galaxy and rejected from our catalog by the FWHM criterion, though they appear to be UDGs. Our method failed to identify them as UDGs. This deblending effect may introduce a bias in our Subaru-UDG samples to more relaxed systems. In other words, our catalog is incomplete to those very extended and irregular galaxies.

5.1.3. Iglesias-Páramo et al. (2003)

Iglesias-Páramo et al. (2003) presented an r-band catalog of the Coma and Abell 1367 clusters. The Coma catalog includes 5555 galaxies, and 92 Subaru-UDGs are found in the catalog. Five DF-UDGs (DF12, DF21, DF23, DF26, and DF28) were found in Iglesias-Páramo et al. (2003).

5.1.4. Adami et al. (2006a)

Adami et al. (2006a) presented $BVRI$ photometry of 60,588 galaxies in the Coma cluster fields. We noticed that the catalog has an offset in the celestial coordinate by several arcseconds in some regions. The offset is checked carefully by eyeball inspection and we identified 248 Subaru-UDGs in the catalog, which include 11 DF-UDGs (DF10, DF12, DF14, DF15, DF18, DF20, DF23, DF25, DF26, DF28, and DF29).

Based on the Adami et al. (2006a) catalog, Adami et al. (2006b) investigated 735 faint LSBs (fLSBs). The UDGs have, however, small overlap with Adami et al. (2006b); only 18 Subaru-UDGs are listed in the catalog, and no DF-UDGs. Of the 18 Subaru-UDGs, 11 have a good GALFIT result.

One of the reasons would be their magnitude criterion, $R > 21$ mag. Since the SB of UDGs and their fLSBs are comparable, the criterion would have removed large LSBs, such as UDGs. They wrote that "fLSB radii range in $\sim 0.17 \leqslant \sigma \leqslant 0.66$ kpc." And actually MW-sized ($r_e \geqslant 1.5$ kpc) galaxies are few, only one, in their catalog. It is a difference of catalog selection criteria; Adami et al. (2006b) focused on more compact galaxies rather than the extended ones like UDGs, and therefore their catalog did not include most UDGs.

5.1.5. Hoyos et al. (2011)

The Advanced Camera for Surveys (ACS) Treasury Survey of the Coma cluster of galaxies (Carter et al. 2008; Hammer et al. 2010; Hoyos et al. 2011) presented HST/ACS images and catalogs of the Coma cluster in F415W and F814W bands.[9] Hoyos et al. (2011) presented structural parameters of 8832 galaxies using GALFIT to ACS F814W images. We searched counterparts of UDGs, and found 36 candidates within three arcseconds from Subaru-UDGs. Meanwhile, no DF-UDG counterpart is found. Three of the Subaru-UDG are deblended too much, and five of them are fit to an off-center bright feature. Among the remaining 28 objects, 18 have good GALFIT results using the Subaru image.

5.1.6. Yamanoi et al. (2012) and Yagi et al. (2010)

Yamanoi et al. (2012) studied the luminosity function (LF) using their unpublished photometric catalog in B- and R-bands. The catalog is based on imaging with Suprime-Cam during

---

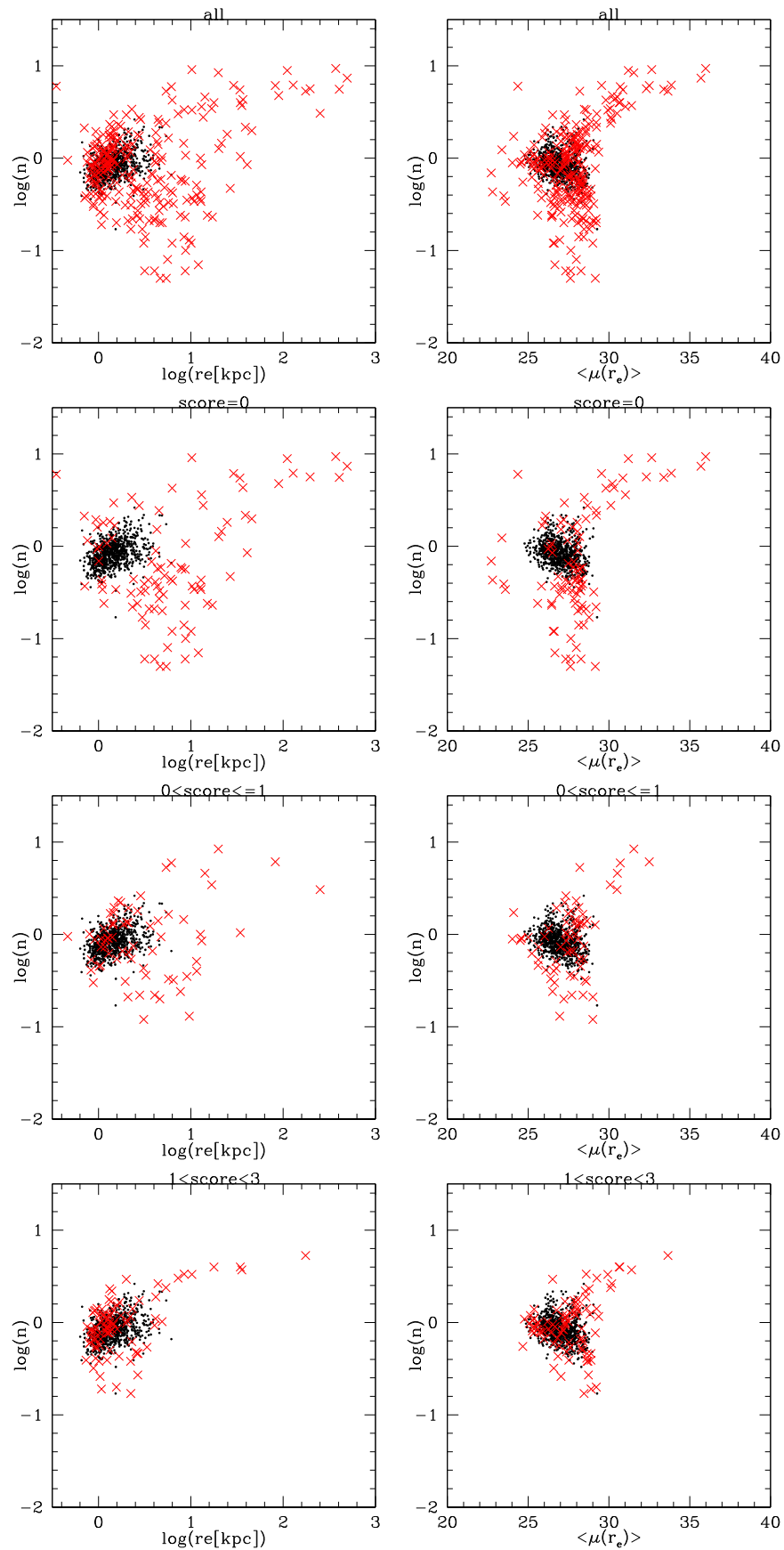[9] http://archive.stsci.edu/prepds/coma/

Figure 12. GALFIT parameters plot of UDGs and objects rejected by eyeball inspection. Filled black dots and red Xs represent UDGs and rejected objects, respectively. The top panels show all the rejected objects, while the other three rows show the rejected objects classified by its score; 0, 0 < score ⩽ 1, and 1 < score < 3, from the top to the bottom. Left: log(r_e) vs. log(Sérsic n) plot. Right: $\langle\mu(r_e)\rangle$ vs. log(Sérsic n) plot.
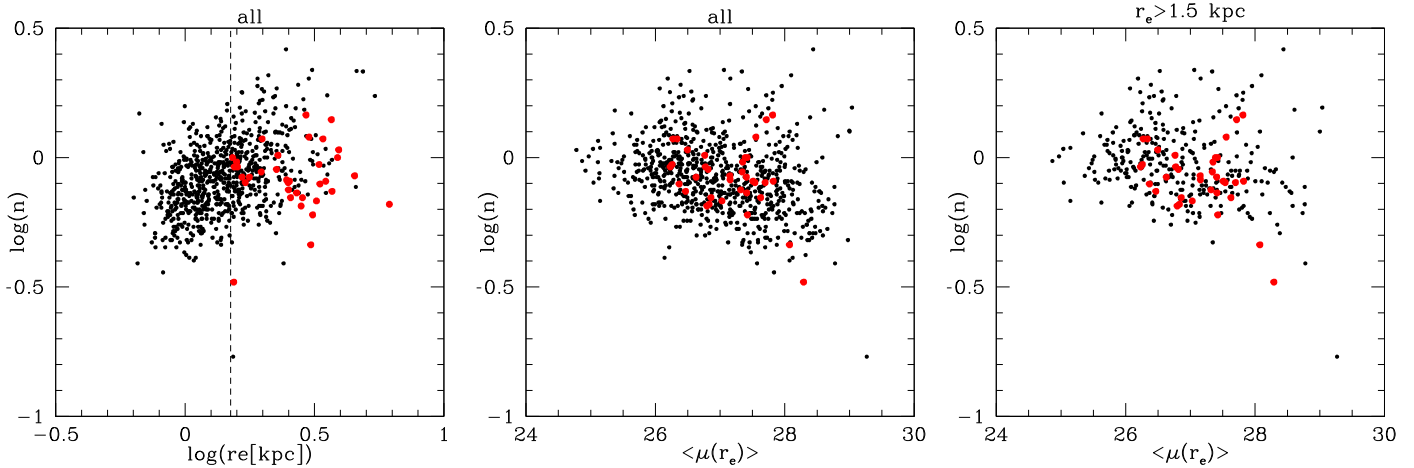
Figure 13. Comparison of Subaru-UDGs (black dots) and DF-UDGs measured in Subaru data (red filled circles). Left: $\log(r_e)$ vs. $\log($Sérsic $n)$ plot. The broken vertical line shows the threshold of GALFIT $r_e = 1.5$ kpc by van Dokkum et al. (2015a). Middle: $\langle \mu(r_e) \rangle$ vs. $\log($Sérsic $n)$ plot. Right: $\langle \mu(r_e) \rangle$ vs. $\log($Sérsic $n)$ plot but the Subaru-UDGs are limited to $r_e > 1.5$ kpc.
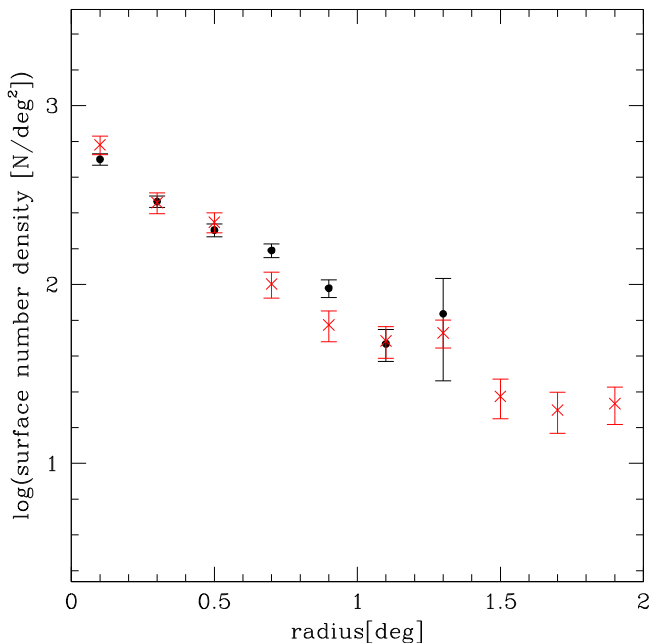
Figure 14. Surface number density profile of Subaru-UDGs in black dots. The error bars show Poisson error. Red crosses show the surface number density profile of giant member galaxies of the Coma cluster selected from SDSS DR7 with an offset of +0.5 dex for comparison with that of the Subaru-UDGs.

2007–2009. We identified Subaru-UDGs and used the $B - R$ color in a fixed two-arcsecond aperture of 232 objects in the catalog.

The $B - R$ color is given in Table 4. Most Subaru-UDGs have color comparable to that of passive galaxies as discussed in Koda et al. (2015).

Yagi et al. (2010) used B, R, i, and narrowband (NA671) images to search for extended ionized clouds in the Coma cluster, while the photometry of each galaxy was not performed. Using the NA671 image, (center, FWHM) = (6710 Å, 120 Å), which corresponds to Hα at the Coma cluster's redshift, we examined whether any visible features of Hα exist in Subaru-UDGs. In 217 postage stamps, no Hα feature was recognized by eyeball inspection.

5.2. Comparison of Measured Parameters

We compared the R-band magnitude by Adami et al. (2006a), Yamanoi et al. (2012), and in this study, and confirmed that our object identification is reasonably good. We also see that there is a slight systematic magnitude difference and flux underestimation by Adami et al. (2006a) for some objects.

Hoyos et al. (2011) gives structural parameters measured with GALFIT in F814W band, and we checked the consistency of our measurement with their catalog. A large difference is seen in n, while other parameters, mag, r_e, and b/a show no significant dispersion. It should be noted that the r_e estimated in this study tend to be smaller than that given by Hoyos et al. (2011). In this sample, there are four MW-sized UDGs, while there are nine with $r_e \geqslant 1.5$ in the Hoyos et al. (2011) catalog. The origin of the difference remains uncertain; it may be the difference of the PSF size, the pixel resolution, the observed wavelength, and/or some parameters for the Sérsic model fitting.

5.3. Parameter Coverage of Previous Catalogs

We plotted the magnitude versus r_e of our measurement, which has counterparts in previous catalogs, in Figure 20. Note that the Subaru-UDGs that we failed to fit with GALFIT are not plotted. In this plot, lower SB is in the top right direction. Godwin et al. (1983) and Iglesias-Páramo et al. (2003) catalogs are the larger and brighter part of the distribution of Subaru-UDGs. They partly overlap with DF-UDGs. Meanwhile, Ulmer et al. (1996), Adami et al. (2006b), and Hoyos et al. (2011) overlap with smaller ($r_e < 2$ kpc) ones. Adami et al. (2006a) and Yamanoi et al. (2012) cover the Subaru-UDG distribution. The difference in the number density would be a smaller size of observed area.

The result shows that at least a part of the Subaru-UDGs were already detected as galaxies and cataloged in the literature, though their structural parameters were not always measured, and therefore they were not recognized as diffuse objects. The importance of a galaxy with a low SB and large extension was also pointed out in previous works (e.g., Penny et al. 2009), but such galaxies tend to have been considered
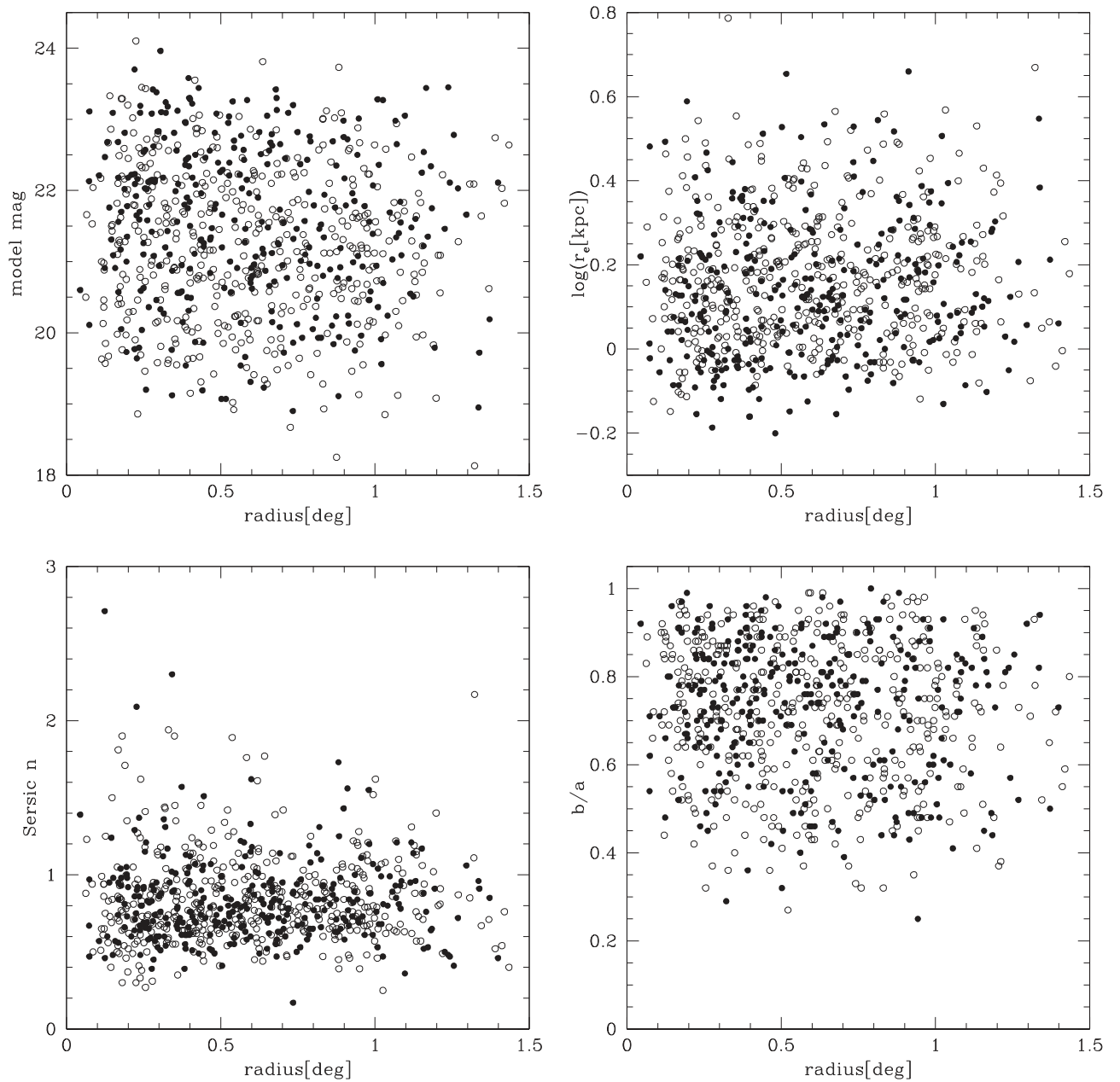
Figure 15. Distance from the center vs. structural parameters from GALFIT. The filled circles are the UDGs for which a single Sérsic component fit is better, and the open circles are the UDGs for which a PSF+Sérsic component fit is better. The parameters of the Sérsic component are given. The ordinates are total model magnitude of the Sérsic component (top left), log of r_e in kiloparsecs (top right), Sérsic n (bottom left), and axis ratio (bottom right), respectively.

5.4. Spectroscopic Catalogs

We checked several redshift catalogs of the Coma cluster field—Mobasher et al. (2001), Smith et al. (2009), Chiboucas et al. (2010, 2011)—and an unpublished redshift catalog by Marzke et al. (in preparation), which is a product of the Survey of the Coma cluster of galaxies collaboration (Carter et al. 2008; Hammer et al. 2010; Hoyos et al. 2011). In these catalogs, six Subaru-UDGs are found. Three of their redshifts are that of a Coma member ($0.015 < z < 0.030$). One has a redshift of a distant object ($z \sim 0.24$), while its appearance implies a chance overlap. The other two do not have a redshift

value in the catalog, but one is classified as a member, and the other is classified as unknown. Recently van Dokkum et al. (2015b) reported that one DF-UDG (DF44) has $z = 0.021$ and identified it as a member of the Coma cluster.

In summary, 854 Subaru-UDGs include five members and no confirmed fore/background objects. Though the fraction of redshift confirmed objects is small, the result is consistent with the statistical discussion by Koda et al. (2015) that the majority of the Subaru-UDGs would be Coma cluster members.

5.5. Comparison with Subaru-UDGs

The Subaru-UDGs were selected to include all DF-UDGs in the SExtractor's output parameter space, and their structural parameters in our catalog were determined using GALFIT after
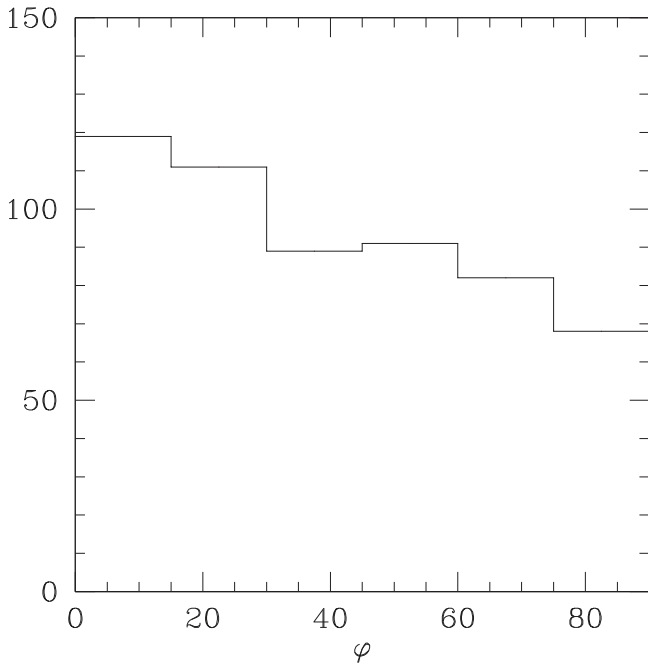
Figure 16. Distribution of the orientation of UDGs' major axis relative to the cluster-centric direction in a 15° bin. UDGs whose b/a is smaller than 0.85 are used. If the major axis aligns in the cluster-centric direction, $\varphi = 0$, and if minor axis aligns to the cluster-centric direction, $\varphi = 90$.
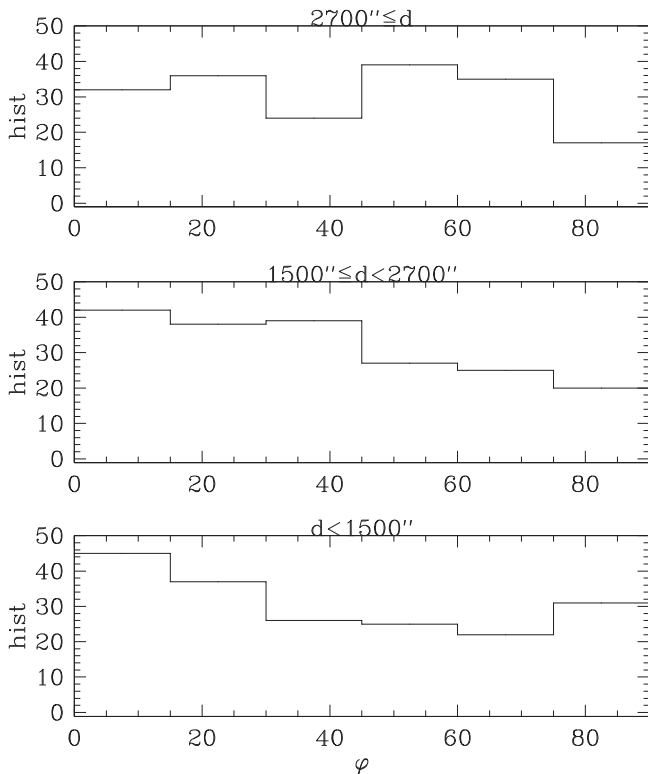

Figure 17. Same as Figure 16, but divided into three according to the projected distance to the cluster center.

Figure 18. Nucleation fraction of Subaru-UDGs as a function of absolute magnitude. The absolute magnitude is based on SExtractor total magnitude (Kron-magnitude) for a comparison with previous studies. Only Poisson error is considered for the error bars.
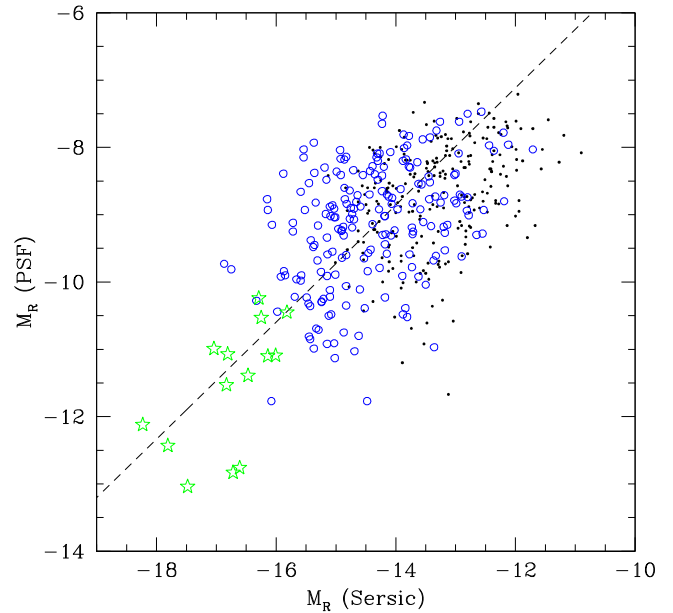
Figure 19. Absolute magnitude of the Sérsic component and the PSF component in PSF+Sérsic models. Blue open circles are MW-sized, and black dots are others. Green stars show the Coma dE,N data in Graham & Guzmán (2003) in the F606W band, and the broken line shows the correlation of the data.

the selection. Hence, not all Subaru-UDGs satisfy the definition of UDGs by van Dokkum et al. (2015b); $r_e > 1.5$ kpc and $\mu_0 > 24$ g mag arcsec^{-2} from an $n = 1$ Sérsic model fitting by GALFIT. If we assume that a typical color of UDG is $g - R = 0.5$, the SB criteria is $\mu_0 > 23.5$ R mag arcsec^{-2}.

In Koda et al. (2015) the number of $r_e > 1.5$ kpc Subaru-UDGs are 334, which was based on GALFIT fits with the single Sérsic model after masking overlapping objects. Their masks were mostly from SExtractor's deblending algorithm, but some were made manually particularly for nuclei. In this work, we did not adopt a manual masking but introduced a PSF +Sérsic model fit.

If we strictly apply the size and SB criteria to Subaru-UDGs, the number of UDGs is 278; 107 objects were fit well with the
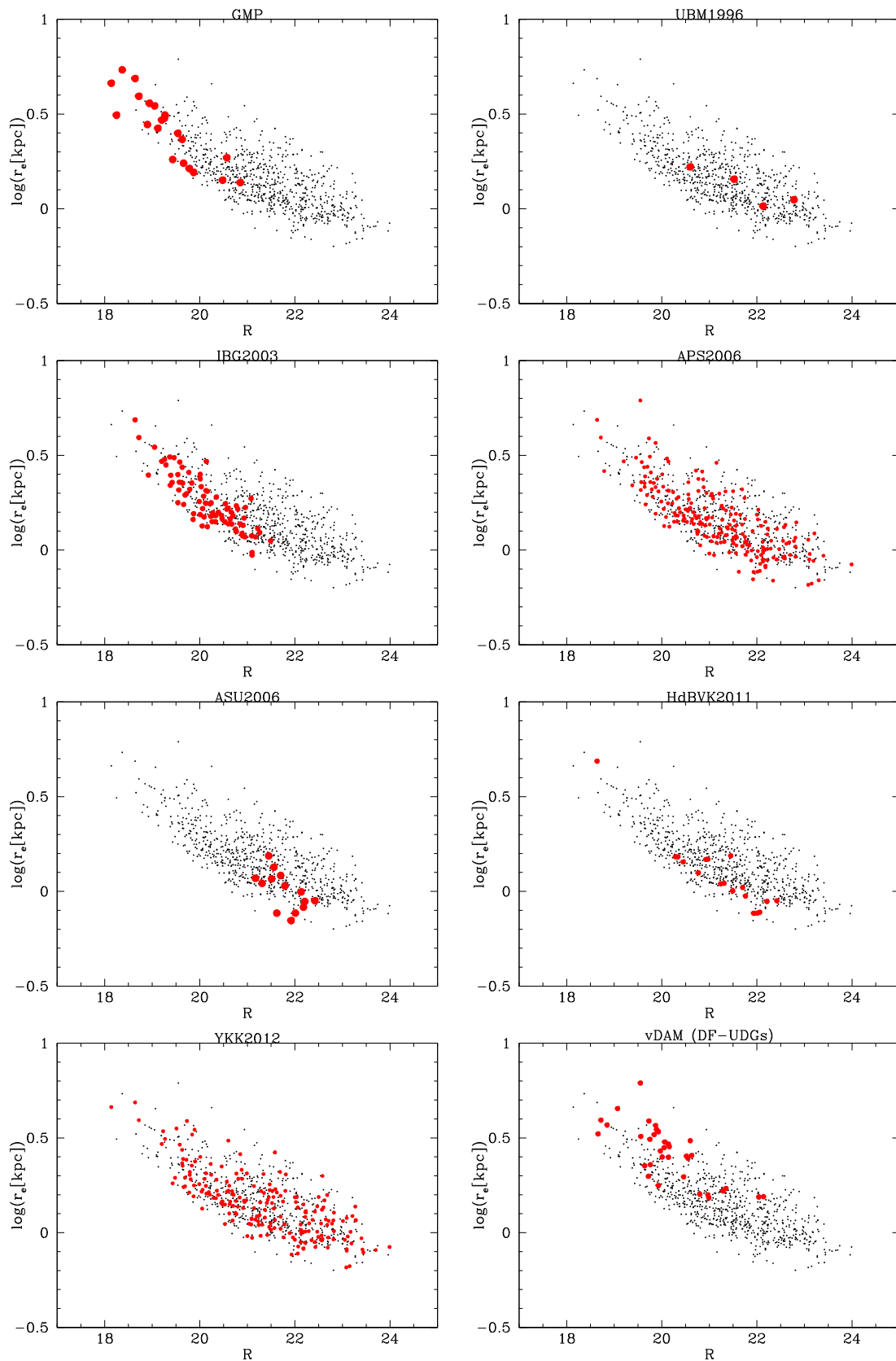
Figure 20. Magnitude vs. r_e plot of Subaru-UDGs with good GALFIT results. The Subaru-UDGs that were also cataloged in previous catalogs are shown as red filled circles. Godwin et al. (1983), Ulmer et al. (1996), Iglesias-Páramo et al. (2003), Adami et al. (2006a), Adami et al. (2006b), Hoyos et al. (2011), Yamanoi et al. (2012), and van Dokkum et al. (2015a) are shown from the left to the right and from the top to the bottom. The magnitude and r_e are taken from our best-fit model with GALFIT.

Sérsic model alone and satisfy $r_e > 1.5$ kpc and $\mu_0 > 23.5\,R$ mag arcsec^{-2}; another 171 objects were fit well with the Sérsic +PSF model, having $r_e > 1.5$ kpc and $\langle\mu(r_e)\rangle > 24.5\,R$ mag arcsec^{-2}. The number of UDGs in this study is still about an order larger than previous studies as shown in Appendix B.

The parameters, r_e and μ_0 (or $\langle\mu(r_e)\rangle$), seem to be smoothly distributed from other LSBs. The definition of UDGs and the threshold for their selection are arbitrary so far, and the question remains as to whether UDGs are a distinct population from other LSB galaxies. The threshold for UDG selection should be investigated with a much larger sample that includes regular LSB galaxies.

6. DISCUSSION

6.1. Statistics of Foreground/Background Objects

We estimated the number of possible foreground/background objects among the 854 Subaru-UDGs using the SDF field as a reference background field. The SDF data has the same field of view (FOV) and depth as those of each of the 18 Suprime-cam fields of the Coma cluster, and the selection of UDGs was made with the same criteria based on the SExtractor parameters. Hence, the number of foreground/background objects in the SDF and each Coma field should follow the same statistics. This study, as in Koda et al. (2015), found no UDG in the comparison SDF field, suggesting that the majority of the Subaru-UDGs are associated with the Coma cluster. In fact, the UDGs-to-giants ratio appears much higher in the Coma cluster than in our neighborhood (Koda et al. 2015). We note that the estimates of their physical scales depend on their distances. If a Subaru-UDG turns out to be a foreground object it would not be classified as a true UDG as its physical r_e should be smaller than those of the population in the Coma cluster. The above comparison suggests that the chance of finding a field UDG within our FOV, though, is very small.

From the non-detection in the reference field, we can set a constraint on the possible number of background objects in the Coma field. If we assume that the number of foreground/background objects follows Poisson statistics, the probability that we will find no UDG in the SDF field is $\exp(-\lambda/f)$, where λ is the mean number of the foreground/background objects in the area of the Coma field size and f is the ratio of the area of the Coma field to the SDF field. The probability distribution function of the number of the foreground/background objects in the Coma field (N) is then calculated as

$$p(N) = a \int d\lambda \exp\left(-\frac{\lambda}{f}\right)\frac{\lambda^N \exp(-\lambda)}{N!} = a\left(\frac{f}{1+f}\right)^{N+1},$$

(9)

where a is the normalization factor and calculated to be $a = 1/f$. The cumulative probability is

$$p(\leqslant N) = \sum_{n=0}^{N} \frac{f^n}{(1+f)^{n+1}} = 1 - \left(\frac{f}{1+f}\right)^N.$$

(10)

As $f \sim 15$ in this study, the 90% confidence range is $N \lesssim 35$. This statistical estimation suggests that the vast majority (96%) of the 854 Subaru-UDGs in the Coma cluster field would be cluster members.

6.2. Dark Matter Fraction

The estimation of the dark matter content from the size and the position of a dwarf galaxy was first proposed by Penny et al. (2009), assuming smoothness and symmetry. With similar methods, van Dokkum et al. (2015a) and Koda et al. (2015) discussed that a high dark matter fraction (fDM) is expected for Coma UDGs. They estimated fDM > 98% (van Dokkum et al. 2015a) and fDM > 99% (Koda et al. 2015) for UDGs, respectively.

The tidal mass inequality is given as Equation (5) of Penny et al. (2009). If we adopt the ellipticity of the orbit $e = 0.5$ (Penny et al. 2009), the pericenter distance $R = 100$ kpc (Koda et al. 2015), the cluster mass within the radius $M_{cl}(R) \sim 3 \times 10^{13}\,M_\odot$ (Łokas & Mamon 2003), and a Petrosian radius of the dwarf $r_d \sim 2.9$ kpc (converted from $r_e = 1.5$ kpc, assuming an exponential profile) for a model UDG in the Coma cluster, the tidal mass is $\sim 3 \times 10^9\,M_\odot$. As the stellar masses of the faintest Subaru-UDGs are $\sim 1 \times 10^7\,M_\odot$ (Koda et al. 2015), fDM $\gtrsim 0.997$ for such UDGs.

The high fDM of >99% has been found in some local dwarf galaxies, especially in ones of small masses and sizes (e.g., Draco and Ursa Minor; Pryor & Kormendy 1990; Trentham et al. 2001). In McConnachie (2012), the dynamical mass and the stellar mass are given for the Local Group dwarfs. The data also show that the fDM of faint LG dwarfs is comparable to that required for Coma UDGs. However, none of these galaxies have a size comparable to the MW.

Such high fDM galaxies (or dark galaxies; Trentham et al. 2001) could resolve/reduce the missing dwarf problem. In the Coma cluster, however, many UDGs were already cataloged in previous studies on the LF (e.g., Adami et al. 2007; Yamanoi et al. 2012). The fraction of newly detected UDGs is only $\sim 0.9\%$ in number, and $\sim 0.3\%$ in flux in the magnitude range of $-16 < M_R < -12$. Even if the mass-to-light ratio (M/L) of UDGs is more than 10 times larger than known dwarfs, the mass fraction of newly detected UDGs is still $\sim 3\%$ of known dwarfs. Meanwhile, the UDGs that are already cataloged in the literature are about 20% of the statistically estimated number of member galaxies in $-16 < M_R < -12$ by Yamanoi et al. (2012). If the M/L of the UDGs is 10 times larger than other dwarfs, the average M/L would be increased by about a factor of three. This is not enough to entirely resolve the missing dwarf problem.

6.3. Radial Alignment and Its Origin

In Section 4.2, we showed that Subaru-UDGs have a radial alignment. The preferential orientation radial alignment may indicate physical processes that are important for the formation and evolution of UDGs.

6.3.1. Radial Alignment in The Coma Cluster in The Literature

The radial alignment of bright galaxies in the Coma cluster were investigated in several studies. Hawley & Peebles (1975) showed that an unusually large fraction has $\varphi \lesssim 45$ among large (angular diameter of the major axis >30 arcsec) galaxies at $600 < d < 3000$ arcsec in the Coma cluster. Their sample selection was the diameter >20 arcsec and the axis ratio $b/a < 0.75$. Thompson (1976) obtained a significant radial trend at a marginal 10% probability level in elliptical galaxies in the Coma cluster. Their sample is selected so that the major axis diameter is larger than $7.5\,h^{-1}$ kpc. They also note that the

other seven clusters do not show the trend. Meanwhile, Torlina et al. (2007) did not detect the radial alignment in galaxies in the central 22.5×29.2 arcmin^2 of the Coma cluster in the catalog by Eisenhardt et al. (2007). Adami et al. (2009) studied galaxies of much fainter magnitude ($18 < R < 24$) in the central 42×52 arcmin^2 of the Coma cluster. They found that there is no radial alignment in most regions, while occasionally a radial alignment is detected in some other regions. They interpret it by collimated infalls or a group merger.

A possible origin of the apparent discrepancy is the sample selection criteria on the size. The studies of the positive results of the radial alignment (Hawley & Peebles 1975, Thompson 1976 and Subaru-UDGs) apply a size criterion, while those of the negative results (Torlina et al. 2007, Adami et al. 2009 and the SDSS DR7 sample in this study) do not. If we limit the SDSS DR7 sample to the galaxies whose isophotal major axes are larger than 10 kpc, and the significance of the radial alignment becomes marginal (p-value is ~ 0.1).

Regarding the change of the radial alignment according to the distance from the center, Faltenbacher et al. (2007) investigated 18,576 groups of galaxies in SDSS DR4 at $0.01 \leqslant z \leqslant 0.2$ whose halo masses are between 5×10^{12} and $5 \times 10^{14}\,M_{\odot}$. They showed that the radial alignment of bright (redshifted to $z = 0.1$ r-band absolute magnitude $M_{0.1r} \leqslant -19 + 5\log h$) galaxies depends on their color; red galaxies show a significant radial alignment where projected distance is smaller than 0.7 of the virial radius (R_{vir}), green ones at $< 0.5\,R_{\mathrm{vir}}$, and no radial alignment of blue galaxies is seen. As the virial radius (R_{vir}) of the Coma cluster is about 2.8 Mpc (Kubo et al. 2007) ~ 6000 arcsec, the radial alignment of Subaru-UDGs is significant in $r/R_{\mathrm{vir}} \lesssim 0.45$, which is comparable to the giant green galaxies in Faltenbacher et al. (2007). Koda et al. (2015) showed that most Subaru-UDGs with available color information have a color comparable to passively evolved galaxies. The UDGs are classified as red or green in the definition by Faltenbacher et al. (2007).

6.3.2. Origin of the Radial Alignment

Several mechanisms have been proposed to make the radial alignment in a cluster, including tidal torque (Ciotti & Dutta 1994; Adami et al. 2009; Pereira & Bryan 2010; Rong et al. 2015a) and primordial alignment (Plionis et al. 2003; Faltenbacher et al. 2007; Rong et al. 2015b).

Primordial alignment is the alignment along large-scale filamentary structures and the alignment to the cluster elongation. If the primordial alignment is effective, the distribution of the radially aligned UDGs should show some anisotropy around the cluster center. The spatial distribution of those UDGs with $b/a < 0.85$ and $\varphi < 15$ is shown in Figure 21. We performed a Kormogorov–Smirnov test of the direction of $b/a < 0.85$ and $\varphi < 15$ UDGs within $d < 2250$ arcsec, where the whole circle is covered by our data. The distribution of the direction of UDGs is shown in Figure 22. In the $d < 2250$ arcsec circle, the azimuthal distribution of radially aligned UDGs ($\varphi < 15$) is not uniform at 95% confidence, while those UDGs with $b/a < 0.85$ and $\varphi \geqslant 15$ in $d < 2250$ arcsec are azimuthally. The anisotropy is strongest around -150 (southwest), where a known substructure (NGC 4839 group) exists. It should also be noted that the alignment in the southwest region is also reported by Adami et al. (2009).

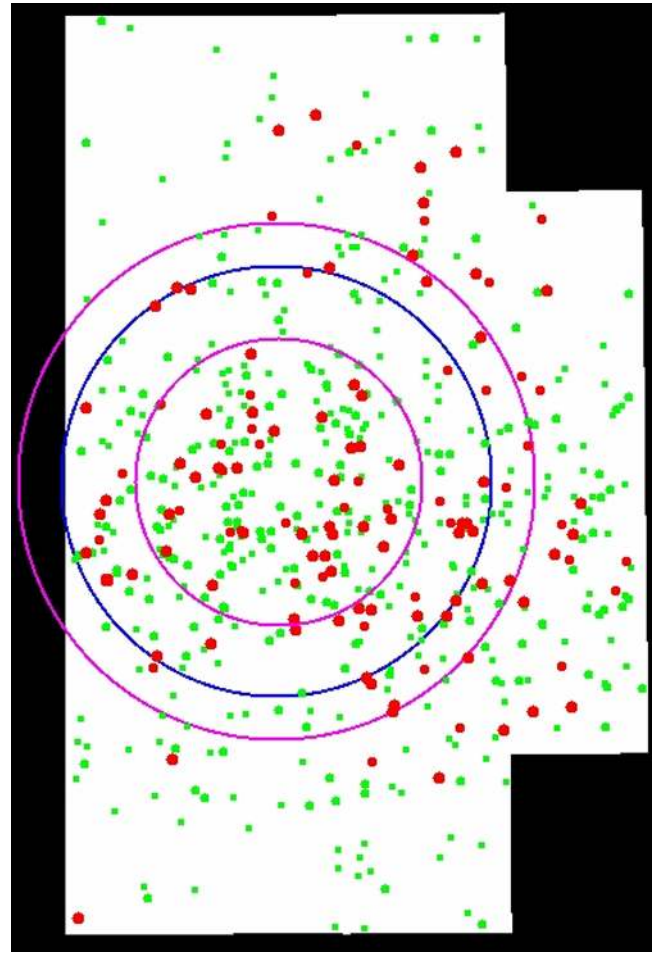Meanwhile, it is difficult to examine with the current data set whether or not the tidal torque also worked. Future

Figure 21. Distributions of UDGs with accurate PA estimation. Green circles show UDGs with $b/a < 0.85$, and red filled circles are UDGs elongated toward the cluster center ($\varphi < 15^{\circ}$). Two magenta circles show the region boundary of Figure 17; $r = 1500$ and 2700 arcsec from the cluster center. The blue circle shows $r = 2250$ arcsec from the cluster center, within which the distribution of azimuthal direction is examined as Figure 22.

spectroscopic study of UDGs will give us partial information about their orbit and may enable us to study the tidal torque statistically.

---

[10] http://smoka.nao.ac.jp/
[11] http://sdss3.org/
[12] http://archive.stsci.edu/
[13] http://hla.stsci.edu/
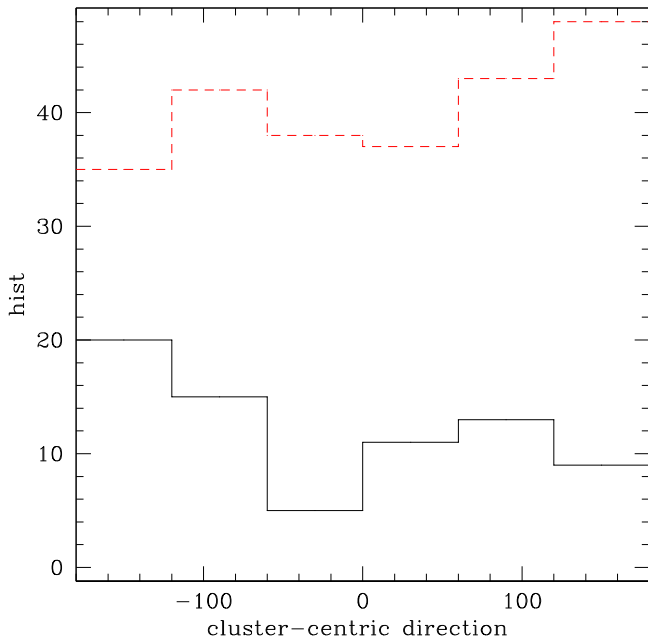[14] http://www4.cadc-ccda.hia-iha.nrc-cnrc.gc.ca/en/

Figure 22. Distribution of the azimuthal direction from the center of the position of UDGs with $b/a < 0.85$ and within $r < 2250$ arcsec (blue circle in Figure 21). The solid black line shows the histogram of UDGs elongated toward the cluster center ($\varphi < 15°$), and the broken red line shows other UDGs.

APPENDIX A
SEXTRACTOR OUTPUT PARAMETERS USED IN THIS STUDY

The SExtractor output parameters used in this study are as follows.

XWIN_IMAGE,YWIN_IMAGE. Pixel coordinate of the center of a detected object.
FLUX_AUTO. Counts in Kron radius.
FWHM. Full-width half maximum from a Gaussian fitting.
PETRO_RADIUS. Petrosian radius. If the luminosity profile of an object is strange, the estimation of the radius fails, and 0 is set to the parameter.
FLUX_RADIUS. Radius in which a certain fraction (FLUX_FRAC) of FLUX_AUTO is included. In this study, we adopted FLUX_FRAC = 0.5, and thus FLUX_RADIUS is the equivalent radius $r_{e,S}$.
MU_EFF_MODEL. The SB at r_e from model fitting. We refer to it as $\mu_{e,S}$.
MU_MEAN_MODEL. The mean SB within r_e. We refer to it as $\langle\mu(r_{e,S})\rangle$.
FLAGS. Flags that indicate saturation, truncation at the edge of the image, deblending failure, etc.

Some parameters used in this study were derived as follows.

1. R.A. and decl. were converted from X_IMAGE and Y_IMAGE with WCSTools (Mink 2002).
2. *R*-band magnitude (*R*) was calculated from FLUX_AUTO as ZP-2.5 log(FLUX_AUTO), where ZP is the magnitude zero point of the image.

Adding to that, the following ellipse parameters were used for the initial parameter for GALFIT.

A_IMAGE. Semimajor axis of ellipse fitting.
B_IMAGE. Semiminor axis of ellipse fitting.
THETA_IMAGE. PA of ellipse fitting.

Also, the following parameters were used for the selection of stars to construct the PSF.

CLASS_STAR. Stellarity index from a neural network classifier (Bertin & Arnouts 1996). If the parameter is large, the probability is high that the object is a star.
FLUX_MAX. The largest pixel count of the object. We adopted $2000 < $ FLUX_MAX $ < 30{,}000$ for this study.

APPENDIX B
MILKY-WAY-SIZED UDGs IN THE LITERATURE

As mentioned in Section 1, UDGs are a subset of LSBs. We can find some galaxies which satisfy the UDG criteria in previously published LSB catalogs, though their numbers are very small compared to the current study. Here we summarize the UDGs we found in the literature. Those catalogs were made with different photometric filters (*B*, *g*, *V*, *R*, and *I*), photometric zero-point systems (Vega versus AB magnitudes), and different parameters (e.g., μ_0, μ_e, or $\langle\mu(r_e)\rangle$). We, therefore, have to make a choice in our definition of UDGs. From Koda et al. (2015), we assume that the UDGs follow the red sequence and have exponential light profiles. For the central SB μ_0 criterion for UDG-like galaxies, we adopted a simple criterion $\mu_0 \gtrsim 24.5$ (*B*), 24 (*g*), 24 (*V*), 23.5 (*R*), or 23.5 (*I*) ABmag arcsec^{-2}, with ~0.5 mag accuracy. For μ_e and $\langle\mu(r_e)\rangle$ catalogs, we used $\mu_e = \mu_0 + 2$ and $\langle\mu(r_e)\rangle = \mu_0 + 1$. For the correction of the magnitude system, we assumed AB-Vega $= -0.1$, 0, 0.2, and 0.45 for *B*, *V*, *R*, and *I*, respectively. Since the μ_0 criterion we adopted is ~0.5 mag accuracy, the offset less than ~0.25 mag is negligible, and only the *I*-band is

Table 5
Number of UDG-like Galaxies in Group/Clusters

Group/Cluster	Reference	# of MW-sized UDGs	μ Criterion
Local Group	McConnachie (2012)	2	$\mu_0 > 24\ V$
NGC 5044 Group	Buzzoni et al. (2012)	3	$\mu_0 > 24\ g$ or $\mu_0 > 24\ V$
NGC 3414 Group	Makarov et al. (2015)	1	$\mu_0 > 23.5\ V$
NGC 5371 Group	Makarov et al. (2015)	1	$\mu_0 > 23.5\ V$
Virgo Cluster	Sandage & Binggeli (1984)	(20)[a]	$\mu_0 > 25\ B$(Vega)
Virgo Cluster	Impey et al. (1988)	11	$\mu_0 > 24\ V$(Vega)
Virgo Cluster	Impey et al. (1988)	5	$\mu_0 > 24.5\ B$(Vega)
Virgo Cluster	Binggeli & Cameron (1993)	8	$\mu_0 > 24.5\ B$(Vega)
Virgo Cluster	Binggeli & Jerjen (1998)	6	$\mu_0 > 24.5\ B$(Vega)
Virgo Cluster	Gavazzi et al. (2005)	11	$\mu_0 > 24.5\ B$(Vega)
Virgo Cluster	Lieder et al. (2012)	3	$\langle \mu(r_e) \rangle > 24.5\ V$
Virgo Cluster	Mihos et al. (2015)	(3)[b]	$\mu_0 > 27\ V$
Fornax Cluster	Muñoz et al. (2015)	6	$\langle \mu(r_e) \rangle > 24\ i$
Abell 1367	Davies et al. (1988)	1	$\mu_0 = 26.2\ R$(Vega)
Pegasus Cluster	Bergmann et al. (2003)	1	$\mu_0 > 24.5\ B$(Vega)
Hydra I Cluster	Misgeld et al. (2008)	1	$\mu_0\ 24\ V$
Coma Cluster	van Dokkum et al. (2015a)	47	$\mu_0 > 24\ g$
Coma Cluster	This work	271[c]	$\mu_0 > 23.5$ or $\langle \mu(r_e) \rangle > 24.5\ R$

Notes.
[a] The size of them is uncertain, though some have large r_e.
[b] The faintest three are reported.
[c] Re-selection based on new results. Note that Koda et al. (2015) mentioned that $r_e > 1.5$ kpc ones are 334, which did not apply any μ_0 criterion.

affected by the difference between the AB and Vega systems. We thus adopted $\mu_0 \gtrsim 23.0\ I$(Vega) mag arcsec^{-2}.

We also adopted a criterion of the half light radius of the disk, $r_e \geqslant 1.5$ kpc, or the exponential scale length $r_d \geqslant 0.9$ kpc for the size criterion. The SB and size criteria correspond to MW-sized Subaru-UDGs. We will limit the sample to $z \lesssim 0.05$ so that the cosmological dimming is negligible in ~ 0.5 mag accuracy. The UDGs found in the literature are summarized in Table 5.

B.1. Field

Nearly 30 years ago, Bothun et al. (1987) reported the discovery of a huge LSB with $\mu_0 = 25.5\ V$ mag arcsec^{-2} and scale length of $r_d = 55\ h^{-1}$ kpc. Its $B - V$ color 0.90 ± 0.02 was 20″ in diameter. This object, later known as "Malin 1," is thought to be an extreme example of a LSB giant spiral galaxy. It satisfies the UDG criteria.

McGaugh & Bothun (1994) gave a multiband surface photometry of 20 LSB disk galaxies. Though most of them have much brighter μ_0, UGC 9024 ($\mu_0 = 24.47\ B$ (Vega) mag arcsec^{-2}) barely satisfy $\mu_0 \geqslant 24.5\ B$ (Vega) mag arcsec^{-2} and the disk scale length of 5.6 kpc satisfies $r_d \geqslant 0.9$ kpc.

Impey et al. (1996) presented a catalog of LSBs at z $\lesssim$ 0.1. The galaxy with $\mu_0 > 24.5\ B$(Vega) mag arcsec^{-2} are 70, 10 of which have redshift information. If we simply convert the redshift to the distance under our adopted cosmological model, 8 satisfy $r_e > 1.5$ kpc.

Dalcanton et al. (1997) discovered seven dwarfs whose exponential scale length $r_d = 1.7$–$3.6\ h_{50}^{-1}$ kpc. Three of them have $\mu_0 \gtrsim 24\ V$ mag arcsec^{-2}, and are comparable to UDGs.

Kniazev et al. (2004) searched for LSBs in the SDSS Early Data Release (Stoughton et al. 2002). They presented 11 giant LSB spiral galaxies with $r_d > 7$ kpc, and five of them satisfy $\mu_0 \gtrsim 24.5\ B$ mag arcsec^{-2}.

Hunter & Elmegreen (2006) gave a catalog of nearby irregular galaxies. Among the 184 irregulars, 6 satisfy $\mu_0 > 24\ V$ mag arcsec^{-2} and $r_e \geqslant 1.5$ kpc. It means that the galaxies selected by the UDG criteria may include irregular galaxies.

Recently, Martinez-Delgado et al. (2016) found a UDG, DGSAT I, near Messier 31. As the galaxy has a recession velocity of 5450 km s^{-1}, they assumed that the galaxy possibly associates with a filament of the Pisces–Perseus supercluster and $r_e \sim 4.7$ kpc.

The small numbers of previous discoveries suggest that field UDGs are rare. In the μ_0 versus r_e plane, field-UDG-like LSBs exist at the tail of the distribution of LSBs. Figure 23 left compares the distributions of LSBs (by the definition of Impey et al. 1996) and of UDGs (LSBs that satisfy the UDG criteria).

NGC 4449B appeared as a UDG, but turned out to be a transient stage of tidal disruption (Rich et al. 2012). The galaxy has $r_e = 2.7$ kpc, and μ_0 is fainter than 25 V mag arcsec^{-2} in their figure, and satisfy the UDG criteria. In this study, however, we removed such possible tidal tails from the catalog by eyeball inspection.

B.2. Cluster and Groups

In addition to the field population, UDGs in a cluster/group environment have also been reported.

B.2.1. Virgo Cluster

The Virgo cluster is the best-studied cluster. About 30 years ago, Sandage & Binggeli (1984) reported ~ 20 galaxies of very low SB ($\mu_0 > 25\ B$(Vega) mag arcsec^{-2}) and of huge size (typically 90 arcsec in diameter) in the Virgo cluster. If we
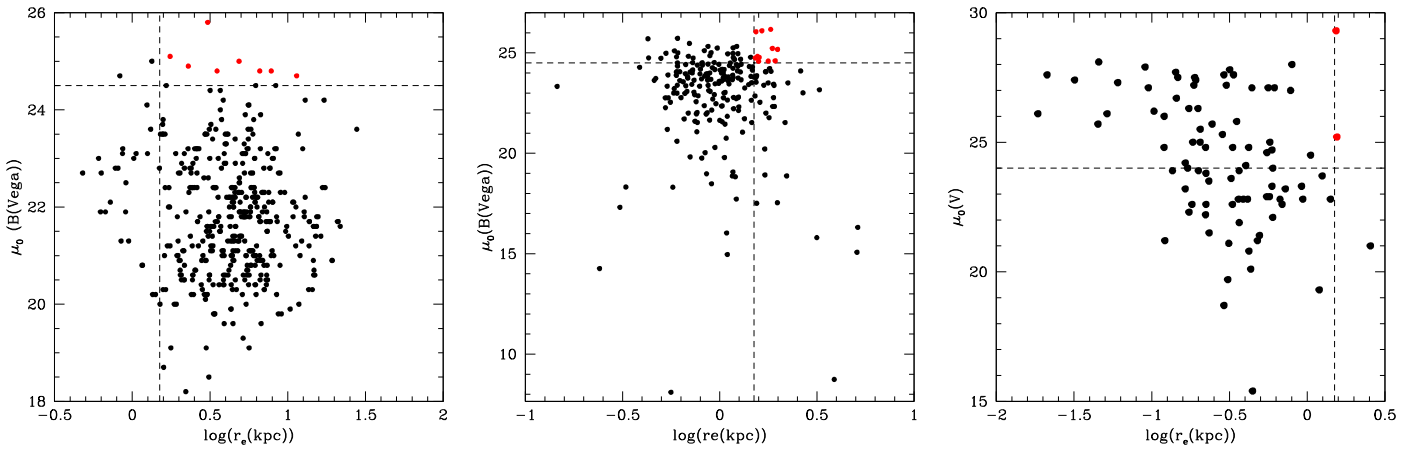
Figure 23. Log(r_e) vs. μ_0 plot of galaxies in various environments. Left: Field galaxies from Impey et al. (1996). The r_e(kpc) is calculated from r_e(arcsec) and the recession velocity given in the catalog. The broken lines show UDG criteria; the horizontal line is $\mu_0 = 24.5$ B(Vega) mag arcsec^{-2}, and the vertical line is $r_e = 1.5$ kpc. Red points represent those which satisfy the UDG criteria. Middle: same as the left but of elliptical galaxies in the Virgo cluster studied by Gavazzi et al. (2005). The distribution in the $r_e - \mu_e$ plane is shown in the middle of Right: Same as the left but of galaxies in the Local Group given by McConnachie (2012). The r_e(kpc) is calculated from R_1(arcmin) and D(kpc), and corrected for b/a. The horizontal line is $\mu_0 = 24$ V mag arcsec^{-2}.

adopt 16.5 Mpc for the distance to the Virgo cluster (Mei et al. 2007), the diameter of 90 arcsec corresponds to 7.2 kpc.

Impey et al. (1988) measured structural parameters of Virgo dwarfs and showed that 27 new galaxies have unusually low SBs and large sizes. The number of galaxies that satisfy $r_d > 0.9$ kpc and either $\mu_0 > 24$ V(Vega) mag arcsec^{-2} or $\mu_0 > 24.5$ B(Vega) mag arcsec^{-2} are 11 (V) and 5 (B), respectively. Three of them are investigated by O'Neil et al. (1999) with WFPC2/HST in the F814W band and all three are old and dynamically relaxed systems and relatively metal-poor.

Binggeli & Cameron (1993) fitted an exponential disk model to the luminosity profiles of dwarf galaxies in the Virgo cluster. Assuming 0.08 kpc arcsec^{-1} for the Virgo cluster, eight galaxies satisfy $r_d > 0.9$ kpc and $\mu_0 > 24.5$ B (Vega) mag arcsec^{-2}. Three of them are classified as nucleated. Binggeli & Jerjen (1998) re-fit those profiles with a Sérsic model. Six dEs satisfy $r_d > 0.9$ kpc ($\log(r_d[\text{arcsec}]) > 1.05$) and $\mu_0 > 24.5$ B(Vega) mag arcsec^{-2}, and three of them are nucleated.

Gavazzi et al. (2005) presented a B-band catalog of elliptical galaxies in the Virgo cluster. Eleven galaxies satisfy $r_e > 1.5$ kpc ($r_e > 19$ arcsec) and $\mu_0 > 24.5$ B (Vega) mag arcsec^{-2}. Three of them are nucleated. Their distribution in the $r_e - \mu_e$ plane is shown in the middle of Figure 23.

Lieder et al. (2012) investigated Virgo dwarfs. Their catalog includes two galaxies (VCC884 and VCC987) that have $\langle \mu(r_e) \rangle > 25$ V mag arcsec^{-2} and $r_e \geqslant 1.5$ kpc. Their $V - I$ (Vega) colors are 1.011 ± 0.018 and 0.819 ± 0.032.

Recently, Mihos et al. (2015) found quite low SB ($\mu_0 > 27$ V mag arcsec^{-2}) galaxies in the Virgo cluster, and Boselli et al. (2016) noted that UDGs are easily detected in the Virgo cluster by the NGVS survey (Ferrarese et al. 2012). In Figure 15 of Ferrarese et al. (2012), images of galaxies of $24.3 < \mu_e < 28.8$ g mag arcsec^{-2} are shown as an example. Some of they may satisfy $\mu_e > 26$ g mag arcsec^{-2}.

B.2.2. Other Clusters

Davies et al. (1988) reported a galaxy (GP1444a Davies et al. 1989) with a $\mu_0 = 26.2$ R(Vega) mag arcsec^{-2} disk in a direction of Abell 1367. If the galaxy is a member of Abell

1367, and 0.45 kpc arcsec^{-1} at the cluster, its scale length ($r_d = 22$ arcsec) corresponds to $r_d = 9.9$ kpc.

O'Neil et al. (1997) surveyed LSBs in the Cancer and Pegasus clusters and also out of clusters near the Great Wall. O'Neil et al. (2000) measured their HI velocity, and Bergmann et al. (2003) presented a compilation of the measurements with recalculations of μ_0 and r_e. In the table, one galaxy in the Pegasus (P9-4) satisfies $\mu_0 > 24.5$ B(Vega) mag arcsec^{-2} and $r_e > 1.5$ kpc.

Misgeld et al. (2008) presented a dwarf catalog in the Hydra I cluster. If $m - M = 33.07$ (Mieske et al. 2005) is adopted, the scale is 0.20 kpc arcsec^{-1}, and only HCC87 satisfies $\mu_0 > 24$ V mag arcsec^{-2} and $r_e \geqslant 1.5$ kpc. Its $V - I$(Vega) colors are 1.07. HCC87 is also investigated by Koch et al. (2012).

In the Fornax cluster, Muñoz et al. (2015) presented a catalog of dwarfs and six (FCC123, FCC130, FCC171, FCC226, FCC233, and FCC272) satisfy $\langle \mu(r_e) \rangle > 24.5$ i mag arcsec^{-2} and $r_e > 1.5$ kpc, which were in the Fornax cluster catalog (FCC; Ferguson 1989). FCC171 is nucleated, while the others are not.

We can also identify UDG candidates by looking at some figures in the literature though many of their parameters have not been published in a tabulated form. In the Antlia cluster (Calderón et al. 2015), we find that some galaxies satisfy $\langle \mu(r_e) \rangle > 25$ V mag arcsec^{-2} and $r_e \gtrsim 1.5$ kpc.

B.2.3. Groups

Carrasco et al. (2001) studied the Dorado Group. In their catalog, three galaxies (L01, L02, and L04) satisfy $r_e > 1.5$ kpc ($r_e > 18$ arcsec) and $\mu_0 > 23$ V mag arcsec^{-2}, assuming that the Dorado group is at 17.2 Mpc distance.

Buzzoni et al. (2012) studied faint galaxies in the NGC 5044 group. If we adopt $m - M = 32.58$ (Buzzoni et al. 2012), the scale is 0.16 kpc arcsec^{-1}, and two (N93A, N156) satisfy $\mu_0 > 24$ g mag arcsec^{-2} and $r_e \geqslant 1.5$ kpc. Their $g - r$ colors are 0.295 and 0.249 in $\mu = 27$ g mag arcsec^{-2} isophote, which is comparable to G5 stars (from their Figure 6). Also one (N62) satisfies $\mu_0 > 24$ V mag arcsec^{-2} and $r_e \geqslant 1.5$ kpc. Its color is $B - V$(Vega) = 1.266 in $\mu = 27$ V mag arcsec^{-2} isophote.

McConnachie ([2012](#)) presented the list of the Local Group galaxies. The galaxies that satisfy $\mu_0 > 24\,V\,\text{mag arcsec}^{-2}$ and $r_e \geqslant 1.5\,\text{kpc}$ are Sagittarius dSph and Andromeda XIX. Their distribution in the r_e–μ_e plane is shown in the right panel of Figure [23](#).

Makarov et al. ([2015](#)) reported three very low SB galaxies outside of the Local Group, and two of them (KKH65 and KK227) satisfy $\mu_0 > 24\,V\,\text{mag arcsec}^{-2}$ and $r_e > 1.5\,\text{kpc}$. KKH65 is a probable member of the NGC 3414 group, and KK227 most likely belongs to the NGC 5371 group (Makarov et al. [2015](#)). Their $V - I$(Vega) colors are 0.93 and 1.17.

REFERENCES

Abazajian, K. N., Adelman-McCarthy, J. K., Agueros, M. A., et al. 2009, ApJS, 182, 543
Abraham, R. G., & van Dokkum, P. G. 2014, PASP, 126, 55
Adami, C., Durret, F., Mazure, A., et al. 2007, A&A, 462, 411
Adami, C., Gavazzi, R., Cuillandre, J. C., et al. 2009, A&A, 493, 399
Adami, C., Picat, J. P., Savine, C., et al. 2006a, A&A, 451, 1159
Adami, C., Scheidegger, R., Ulmer, M., et al. 2006b, A&A, 459, 679
Adelman-McCarthy, J. K., Agueros, M. A., Allam, S. S., et al. 2007, ApJS, 172, 634
Ahn, C. P., Alexandroff, R., Allende Prieto, C., et al. 2012, ApJS, 203, 21
Baba, H., Yasuda, N., Ichikawa, S.-I., et al. 2002, in ASP Conf. Ser. 281, ADASS XI, ed. D. A. Bohlender, D. Durand, & T. H. Handley (San Francisco: ASP), 298
Bergmann, M. P., Jørgensen, I., & Hill, G. J. 2003, AJ, 125, 116
Bertin, E., & Arnouts, S. 1996, A&AS, 317, 393
Binggeli, B., & Cameron, L. M. 1993, A&AS, 98, 297
Binggeli, B., & Jerjen, H. 1998, A&A, 333, 17
Binggeli, B., Sandage, A., & Tarenghi, M. 1984, AJ, 89, 64
Blanton, M. R., & Roweis, S. 2007, AJ, 133, 734
Boselli, A., Boissier, S., Voyer, E., et al. 2016, A&A, 585, A2
Bothun, G., Impey, C., Malin, D. F., & Mould, J. R. 1987, ApJ, 291, 586
Buzzoni, A., Callone, S. A., Saracco, P., & Zucca, E. 2012, MNRAS, 420, 3427
Calderón, J. P., Bassino, L. P., Cellone, S. A., et al. 2015, MNRAS, 451, 791
Carrasco, E. R., Mendes de Oliveira, C., Infante, L., & Bolte, M. 2001, AJ, 121, 148
Carrasco, E. R., Mendes de Oliveira, C., Infante, L., & Bolte, M. 2006, AJ, 132, 1796
Carter, D., Goudfrooij, P., Mobasher, B., et al. 2008, ApJS, 176, 424
Chiboucas, K., Tully, R. B., Marzke, R. O., et al. 2010, ApJ, 723, 251
Chiboucas, K., Tully, R. B., Marzke, R. O., et al. 2011, ApJ, 737, 86
Ciotti, L., & Dutta, S. N. 1994, MNRAS, 270, 390
Côté, P., Piatek, S., Ferrarese, L., et al. 2006, ApJS, 165, 57
Dalcanton, J. J., Spergel, D. N., Gunn, J. E., Schmidt, M., & Schneider, D. P. 1997, AJ, 114, 635
Davies, J. I., Phillipps, S., & Disney, M. J. 1988, MNRAS, 231, 69
Davies, J. I., Phillipps, S., & Disney, M. J. 1989, MNRAS, 239, 703
den Brok, M., Peletier, R. F., Seth, A., et al. 2014, MNRAS, 445, 2385
Eisenhardt, P. R., De Propris, R., Gonzalez, A. H., et al. 2007, ApJS, 169, 225
Faltenbacher, A., Li, C., Mao, S., et al. 2007, ApJL, 662, L71
Ferguson, H. C. 1989, AJ, 98, 367
Ferrarese, L., Côteé, P., Cuillandre, J.-C., et al. 2012, ApJS, 200, 4
Gavazzi, G., Donati, A., Cucciati, O., et al. 2005, A&A, 430, 411
Godwin, J. G., Metcalfe, N., & Peach, J. V. 1983, MNRAS, 202, 113
Graham, A. W., & Driver, S. P. 2005, PASA, 22, 118
Graham, A. W., & Guzmán, R. 2003, AJ, 125, 2936
Hammer, D., Verdoes Kleijn, G., Hoyos, C., et al. 2010, ApJS, 191, 143
Hawley, D. L., & Peebles, P. J. E. 1975, AJ, 80, 477
Hinshaw, G., Larson, D., Komatsu, E., et al. 2013, ApJS, 208, 19
Hoyos, C., den Brok, M., Verdoes Kleijn, G., et al. 2011, MNRAS, 411, 2439

Hunter, D. A., & Elmegreen, B. G. 2006, ApJS, 162, 49
Iglesias-Páramo, J., Boselli, A., Gavazzi, G., Cortese, L., & Vílchez, J. M. 2003, A&A, 397, 421
Impey, C., Bothun, G., & Malin, D. 1988, ApJ, 330, 634
Impey, C., Sprayberry, D., Irwin, M. J., & Bothun, G. D. 1996, ApJS, 105, 209
Iye, M., Karoji, H., Ando, H., et al. 2004, PASJ, 56, 381
Kashikawa, N., Shimasaku, K., Yasudan, N., et al. 2004, PASJ, 56, 1011
Kavelaars, J. J., Harris, W. E., Hanes, D. A., et al. 2000, ApJ, 533, 125
Kniazev, A. Y., Grebel, E. K., Pustilnik, S. A., et al. 2004, AJ, 127, 704
Koch, A., Burkert, A., Rich, R. M., et al. 2012, ApJL, 755, L13
Koda, J., Yagi, M., Yamanoi, H., & Komiyama, Y. 2015, ApJL, 807, L2
Kubo, J. M., Stebbins, A., Annis, J., et al. 2007, ApJ, 671, 1466
Lasker, B. M., Lattanzi, M. G., McLean, B., et al. 2008, AJ, 136, 735
Lieder, S., Lisker, T., Hilker, M., Misgeld, I., & Durrell, P. 2012, A&A, 538, 69
Łokas, E. L., & Mamon, G. A. 2003, MNRAS, 343, 401
Makarov, D. I., Sharina, M. E., Karachentseva, V. E., & Karachentsev, I. D. 2015, A&A, 581, A82
Martinez-Delgado, D., Lasker, R., Sharina, M., et al. 2016, AJ, 151, 96
McConnachie, A. W. 2012, AJ, 144, 4
McGaugh, S. S., & Bothun, G. D. 1994, AJ, 107, 530
Mei, S., Blakeslee, J. P., Cote, P., et al. 2007, ApJ, 655, 144
Michard, R., & Andreon, S. 2008, A&A, 490, 923
Mieske, S., Hilker, M., & Infante, L. 2005, A&A, 438, 103
Mihos, J. C., Durrell, P. R., Ferrarese, L., et al. 2015, ApJL, 809, l21
Mink, D. J. 2002, in ASP Conf. Proc. 281, ADASS XI, ed. D. A. Bohlender, D. Durand, & T. H. Handley (San Francisco, CA: ASP), 169
Misgeld, I., Mieske, S., & Hilker, M. 2008, A&A, 486, 697
Miyazaki, S., Komiyama, Y., Sekiguchi, M., et al. 2002, PASJ, 54, 833
Mobasher, B., Bridges, T. J., Carter, D., et al. 2001, ApJS, 137, 279
Muñoz, R., Eigenthaler, P., Puzia, T. H., et al. 2015, ApJL, 813, L15
O'Neil, K., Bothun, G. D., & Impey, C. D. 1999, AJ, 118, 1618
O'Neil, K., Bothun, G. D., & Schombert, J. 2000, AJ, 119, 136
O'Neil, K., Bothun, G. D., Schombert, J., Cornell, M. E., & Impey, C. D. 1997, AJ, 114, 2448
Okabe, N., Futamase, T., Kajisawa, M., & Kuroshima, R. 2014, ApJ, 784, 90
Peng, C. Y., Ho, L. C., Impey, C. D., & Rix, H.-W. 2002, AJ, 124, 266
Peng, C. Y., Ho, L. C., Impey, C. D., & Rix, H.-W. 2010, AJ, 139, 2097
Penny, S. J., Conselice, C. J., de Rijcke, S., & Held, E. V. 2009, MNRAS, 393, 1054
Pereira, M. J., & Bryan, G. L. 2010, ApJ, 721, 939
Plionis, M., Benoist, C., Maurogordato, S., Ferrari, C., & Basilakos, S. 2003, ApJ, 594, 144
Pryor, C., & Kormendy, J. 1990, AJ, 100, 127
Rich, R. M., Collins, M. L. M., & Black, C. M. 2012, Natur, 482, 192
Rong, Y., Yi, S., Zhang, S., & Tu, H. 2015a, MNRAS, 451, 2536
Rong, Y., Zhang, S., & Liao, J. 2015b, MNRAS, 453, 1577
Sandage, A., & Binggeli, B. 1984, AJ, 89, 919
Schlafly, E. F., & Finkbeiner, D. P. 2011, ApJ, 737, 103
Schlegel, D. J., Finkbeiner, D. P., & Davis, M. 1998, ApJ, 500, 525
Sérsic, J. L. 1968, Atlas de Galaxias Australes (Córdoba: Obs. Astron. Córdoba)
Smith, R. J., Lucey, J. R., Hudson, M. J., et al. 2009, MNRAS, 392, 1265
Stoughton, C., Lupton, R. H., Bernardi, M., et al. 2002, AJ, 123, 485
Thompson, L. A. 1976, ApJ, 209, 22
Torlina, L., De Propris, R., & West, M. J. 2007, ApJL, 660, L97
Trentham, N., Möller, O., & Ramirez-Ruiz, E. 2001, MNRAS, 322, 658
Ulmer, M. P., Bernstein, G. M., Martin, D. R., et al. 1996, AJ, 112, 2517
van Dokkum, P. G., Abraham, R., Merritt, A., et al. 2015a, ApJL, 798, L45
van Dokkum, P. G., Romanowsky, A., Abraham, R., et al. 2015b, ApJL, 804, L26
White, S. D. M., Briel, U. G., & Henry, J. P. 1993, MNRAS, 261, L8
Yagi, M. 2012, PASP, 124, 1374
Yagi, M., Suzuki, N., Yamanoi, H., et al. 2013, PASJ, 65, 22
Yagi, M., Yoshida, M., Komiyama, Y., et al. 2010, AJ, 140, 1814
Yamanoi, H., Komiyama, Y., Yagi, M., et al. 2012, AJ, 144, 40